Article

Cancer Cell

Gain Fat—Lose Metastasis: Converting Invasive Breast Cancer Cells into Adipocytes Inhibits Cancer Metastasis

Graphical Abstract

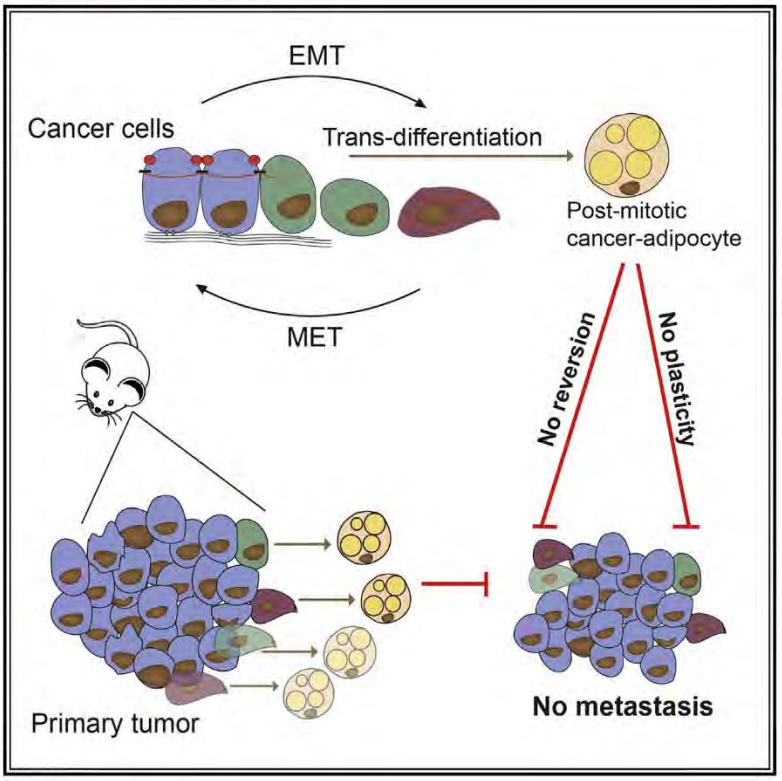

Authors

Dana Ishay-Ronen,
Maren Diepenbruck,
Ravi Kiran Reddy Kalathur, ...,
Junrong Wang, Christoph Hess,
Gerhard Christofori

Correspondence

pandanaro@gmail.com (D.I.-R.),
gerhard.christofori@unibas.ch (G.C.)

In Brief

Ronen et al. show that the cellular plasticity of cancer cells undergoing EMT can be exploited to force trans-differentiation of breast cancer cells into post-mitotic and functional adipocytes, leading to the repression of primary tumor invasion and metastasis formation.

Highlights

- EMT-derived breast cancer cells can differentiate into post-mitotic adipocytes
- Adipogenesis disconnects cancer cells from an invasive and oncogenic phenotype
- EMT/MET transcription factors and TGF-β signaling regulate cancer adipogenesis
- Adipogenesis-inducing drug combinations repress metastasis in preclinical models

Ishay-Ronen et al., 2019, Cancer Cell *35*, 17–32
January 14, 2019
https://doi.org/10.1016/j.ccell.2018.12.002

CellPress

Cancer Cell
Article

CellPress

Gain Fat—Lose Metastasis: Converting Invasive Breast Cancer Cells into Adipocytes Inhibits Cancer Metastasis

Dana Ishay-Ronen,[1,*] Maren Diepenbruck,[1] Ravi Kiran Reddy Kalathur,[1] Nami Sugiyama,[1] Stefanie Tiede,[1] Robert Ivanek,[1] Glenn Bantug,[2] Marco Francesco Morini,[1] Junrong Wang,[1] Christoph Hess,[2] and Gerhard Christofori[1,3,*]
[1]Department of Biomedicine, University of Basel, Mattenstrasse 28, 4058 Basel, Switzerland
[2]University Hospital Basel, Department of Biomedicine, University of Basel, Switzerland
[3]Lead Contact
*Correspondence: pandanaro@gmail.com (D.I.-R.), gerhard.christofori@unibas.ch (G.C.)
https://doi.org/10.1016/j.ccell.2018.12.002

SUMMARY

Cancer cell plasticity facilitates the development of therapy resistance and malignant progression. De-differentiation processes, such as an epithelial-mesenchymal transition (EMT), are known to enhance cellular plasticity. Here, we demonstrate that cancer cell plasticity can be exploited therapeutically by forcing the trans-differentiation of EMT-derived breast cancer cells into post-mitotic and functional adipocytes. Delineation of the molecular pathways underlying such trans-differentiation has motivated a combination therapy with MEK inhibitors and the anti-diabetic drug Rosiglitazone in various mouse models of murine and human breast cancer *in vivo*. This combination therapy provokes the conversion of invasive and disseminating cancer cells into post-mitotic adipocytes leading to the repression of primary tumor invasion and metastasis formation.

INTRODUCTION

Cancer cell plasticity is defined as the capacity of a cell to adapt to dynamic changes, triggered by external signals. Cellular plasticity plays a critical role in cancer cell survival, invasion, and metastasis formation (Massague and Obenauf, 2016), as well as in tumor heterogeneity (Koren et al., 2015; Van Keymeulen et al., 2015) and in the development of therapy resistance (Holohan et al., 2013; Jordan et al., 2016). Cancer cell plasticity is dynamic and can be the result of changing cues in the microenvironment (Oshimori et al., 2015; Puram et al., 2017). An epithelial-mesenchymal transition (EMT) seems to play a major role in facilitating cell plasticity in cancer and allows cancer cells to escape chemotherapies and targeted therapies by de-differentiation and signaling adaption processes (Fischer et al., 2015; Gao et al., 2012; Krebs et al., 2017; Puram et al., 2017; Valiente et al., 2014; Zheng et al., 2015). While EMT is responsible for primary tumor cell invasion, its reversal, mesenchymal-epithelial transition (MET), has been shown to contribute to the metastatic outgrowth of disseminated cancer cells in distant organs (Brabletz et al., 2018; Ocana et al., 2012; Tsai et al., 2012). Hence, the therapeutic reversion of EMT could be counterproductive (Nieto, 2013). However, it has also been noted that cells undergoing EMT and/or MET are in a highly plastic state and thus may offer a window of opportunity for therapeutic targeting (Brabletz, 2012a; Gupta et al., 2009; Nieto, 2013; Nieto et al., 2016; Pastushenko et al., 2018). EMT in non-transformed mammary epithelial cells has also been linked to increased multi-lineage differentiation potential, demonstrating characteristics that resemble mesenchymal stem cells (Battula et al., 2010).

The observation that cell de-differentiation processes in cancer are often correlated with increased malignancy and cancer-metastatic potential (Lawson et al., 2015; Oshimori et al., 2015; Tam and Weinberg, 2013) has readily lead to the appealing strategy of treating malignancies by inducing cancer cell differentiation (de The, 2018; Prost et al., 2015). While attempted already in 1959 as a possible treatment for teratoma (Pierce and Dixon, 1959), a prominent example of a highly successful

Significance

Cancer cell plasticity and EMT are dynamic and can occur during different steps of cancer metastasis. We demonstrate that cellular plasticity acquired by EMT can be exploited to trans-differentiate breast cancer cells into post-mitotic and functional adipocytes. Notably, adipogenic differentiation therapy with a combination of Rosiglitazone and an MEK inhibitor efficiently inhibits cancer cell invasion, dissemination, and metastasis formation in various preclinical mouse models of breast cancer. The results underscore the pivotal role of cancer cell plasticity in malignant tumor progression and reveal the therapeutic potential that lies in the targeting of cellular plasticity, for example by forcing post-mitotic adipogenesis.

differentiation therapy has been the introduction of all-*trans* retinoic acid as a therapy for acute promyelocytic leukemia (de The, 2018). In carcinomas, therapeutic approaches to revert de-differentiated cancer cells into normal epithelial cells have reduced cell proliferation and increased the sensitivity to chemotherapy (Girnun et al., 2007; Mueller et al., 1998; Wielenga et al., 2015). However, as emphasized above, cancer cell plasticity and the dynamic nature of EMT and MET during tumor dissemination and metastatic outgrowth underscore the possible weakness of epithelial re-differentiation. Although these processes are not fully understood, there is growing evidence that inducing MET may enhance metastatic outgrowth (Brabletz, 2012b; Pattabiraman and Weinberg, 2014). A further open question concerns the ability of re-differentiated cancer cells to undergo further phenotypic changes through a second EMT, a possible outcome that would endure plasticity responses (Brabletz et al., 2018).

In this study, we hypothesize that cancer cell plasticity is necessary for cancer dissemination but can be directly targeted and inhibited by a trans-differentiation approach, such as forced adipogenesis.

RESULTS

EMT Breast Cancer Cells Trans-differentiate into Adipocytes

As cellular models of EMT-induced cancer cell plasticity we used Py2T murine epithelial tumor cells derived from a mammary tumor of an MMTV-PyMT transgenic mouse. Py2T cells undergo a reversible EMT upon treatment with transforming growth factor β (TGF-β) *in vitro* and gain mesenchymal characteristics when implanted into mice (Tiwari et al., 2013; Waldmeier et al., 2012). Py2T-LT (LT [long-term treatment]) cells are Py2T cells that have been treated with TGF-β for at least 20 days to induce a complete EMT. As a second experimental system, we employed epithelial MTflECad murine breast cancer cells derived from a mammary tumor of an MMTV-Neu transgenic mouse. MTflECad cells carry conditional (floxed) alleles of the E-cadherin gene (*Cdh1*) and undergo an EMT upon Cre recombinase-mediated ablation of E-cadherin (MTΔECad cells). They represent an irreversible EMT model of murine mammary gland tumor cells with demonstrated cancer stem cell characteristics (Fantozzi et al., 2014; Lehembre et al., 2008).

We employed methods established in the field of adipogenesis (Kopinke et al., 2017; Wang et al., 2014) to test whether EMT-derived breast cancer cells can be induced to undergo adipogenesis. The results were directly compared with 3T3-L1 pre-adipocytic fibroblasts, a cellular adipogenesis model committed to the adipose lineage (Birsoy et al., 2008; Rosen and Spiegelman, 2014; Tontonoz et al., 1994). We first optimized an adipogenesis protocol in 3T3-L1 pre-adipocytes which are well-known to differentiate into adipocytes when induced with insulin, dexamethasone and Rosiglitazone (a potent agonist of peroxisome proliferator-activated receptor γ [PPARγ]) (Gubelmann et al., 2014; Hong et al., 2005; Tontonoz et al., 1994) (Figure 1A). For the induction of adipogenesis in mammary gland tumor cells, this protocol was combined with bone morphogenetic protein-2 (BMP2), as suggested for multipotent mesenchymal stem cell differentiation (Gubelmann et al., 2014; Tseng et al., 2008). The generation of adipocytes, as assessed by visualizing lipid droplets of fluorescent Nile Red, was readily detected in treated mesenchymal breast cancer cells but not in their treated epithelial counterparts (Figure 1A). The expression of C/EBPα, a regulator of adipogenesis expressed in the pre-adipocytic cell line 3T3-L1 during adipogenesis (Lefterova et al., 2008; Rosen et al., 2002), was also present in mesenchymal Py2T-LT and with higher incidence in MTΔECad cells induced to undergo adipogenesis (Figure 1B). The expression of C/EBPα could not be detected in epithelial Py2T or MTflECad cells treated with the differentiation protocol. C/EBPβ, an early regulator of adipogenesis and gatekeeper of adipogenic lineage determination (Birsoy et al., 2008; Raghav et al., 2012), was found absent in untreated and treated epithelial MTflECad cells, yet expressed already in untreated as well as in treated MTΔECad mesenchymal cells (Figure S1A).

We next assessed whether the plasticity of EMT-derived breast cancer cells includes the ability to differentiate into further cell types of the mesenchymal lineage, such as osteoblasts and chondrocytes, as previously demonstrated for non-transformed cells (Battula et al., 2010). MTΔECad cells were treated with differentiation protocols adapted from a previous report on the induction of osteogenesis and chondrogenesis (Nusspaumer et al., 2017). Indeed, osteogenesis-induced cells expressed the osteoblast regulator Osterix (Figure S1B), while chondrogenesis-induced cells expressed chondrocyte-specific collagen type 2 and Sox9, a master transcription factor of chondrogenesis (Figure S1C). The results underscore the high cell plasticity and trans-differentiation potential of mammary gland tumor cells that have undergone an EMT.

To enable adipogenesis of malignant cancer cells as a therapeutic option, we aimed at reducing the treatment protocol to a minimal number of pharmaceutical compounds. The highest efficiency of adipogenesis was found with a combination of Rosiglitazone and BMP2 (data not shown). Thus, all *in vitro* experiments described hereafter were performed according to this optimized protocol (Figure 1C), unless stated otherwise.

Adipogenesis-Induced Cancer Cells Become Functional Post-mitotic Adipocytes

We next investigated whether the adipocytes originating from EMT-derived mammary gland tumor cells represented bona fide adipocytes (Wang et al., 2014). Notably, adipogenesis-induced MTΔECad and 3T3-L1 cells represented functional adipocytes with comparable characteristics. For example, both differentiated cell types express the adipocyte-specific markers C/EPBα, PPARγ2, and fatty acid binding protein 4 (FABP4) (Figure 2A), they secrete the adipocyte-specific adipokine adiponectin (Figure 2B), and they share a metabolic phenotype (Figure S2A). Moreover, lipolysis can be induced by the β-adrenergic agonist isoproterenol in both differentiated adipocytes (Figure 2C). Finally, the insulin-sensitive glucose transporter GLUT4 was translocated to the surface of adipogenesis-differentiated MTΔECad cells upon stimulation with insulin (Figure 2D).

Along with acquiring adipocyte-specific features, EMT-derived adipogenesis-differentiated cancer cells lost their mesenchymal, invasive traits. Visualization of the actin cytoskeleton by Phalloidin staining revealed a reorganization of mesenchymal stress fibers into cortical actin, a hallmark of cell immobilization, even in the absence of E-cadherin expression in MTΔECad cells

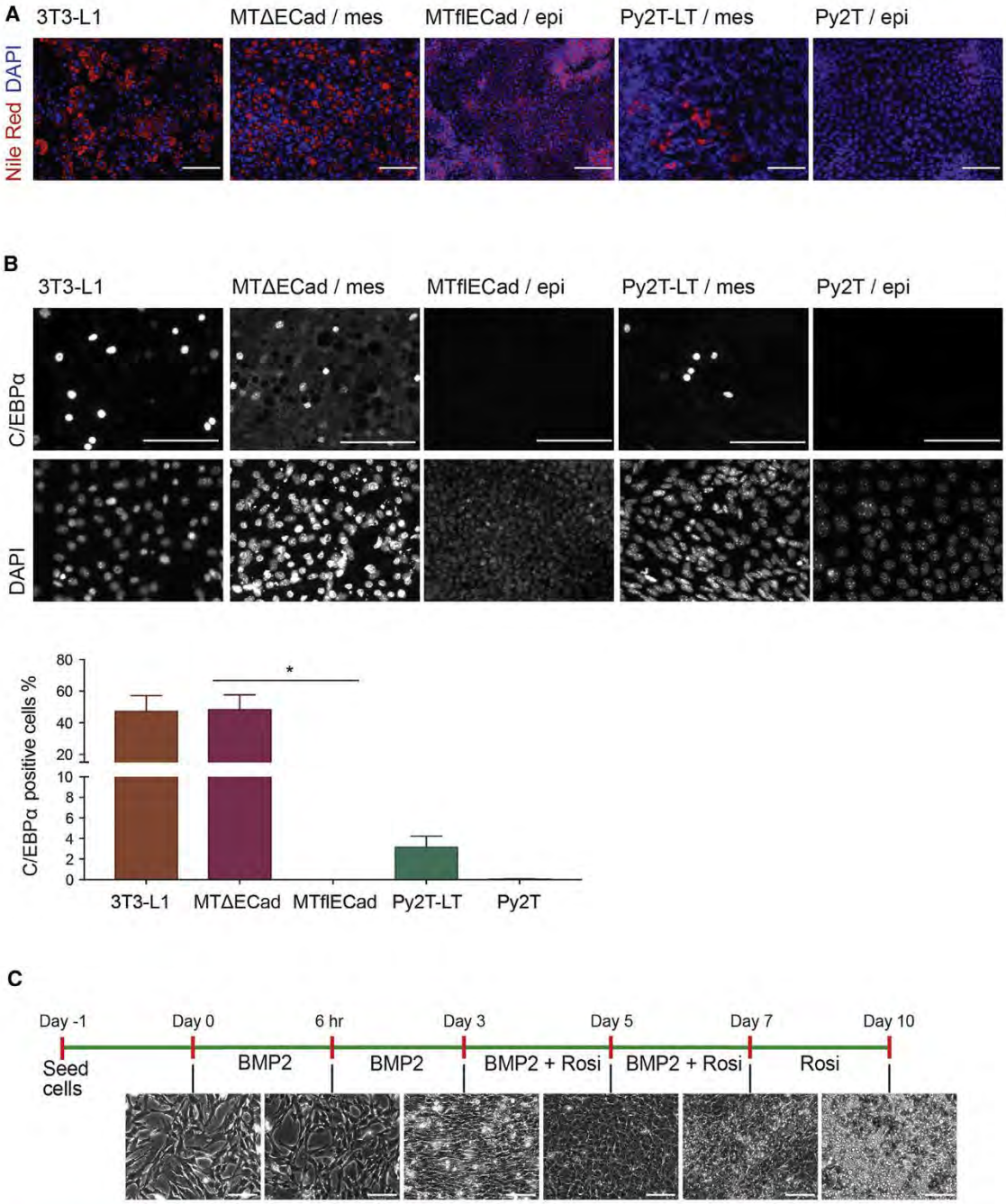

Figure 1. EMT-Derived Breast Cancer Cells but Not Epithelial Cancer Cells Can Be Induced to Differentiate into Adipocytes

(A and B) Fibroblastic pre-adipocytes (3T3-L1) were treated with insulin, dexamethasone, and Rosiglitazone (Rosi) to induce adipogenesis. Mesenchymal (MTΔEcad and Py2T-LT; mes) and epithelial (MTflEcad and Py2T; epi) cancer cells were treated with insulin, dexamethasone, Rosiglitazone, and BMP2 to induce adipogenesis. Lipid droplets were visualized by immunofluorescence microscopy with Nile Red (red), nuclei with DAPI (blue) (A). The adipogenesis regulator C/EBPα was visualized by immunofluorescence microscopy (upper panel) and nuclei by DAPI (lower panel) (B). C/EBPα-positive cells were quantified. Graph shows means ± SEM (n = 3); unpaired Student's t test; *p < 0.0332. Scale bar, 100 μm.

(C) Schematic representation of the optimized *in vitro* treatment protocol and timed microphotographs of MTΔECad cells undergoing forced adipogenesis *in vitro*. Scale bar, 100 μm.

See also Figure S1.

(Figure 2E). Moreover, mesenchymal α-smooth muscle actin expression was reduced, while adiponectin expression was increased in adipogenesis-differentiated MTΔECad cells (Figure S2B). To assess the reversibility of the differentiation process, the differentiation medium was replaced by normal culture medium for 9 days after differentiation treatment. Subsequent Nile

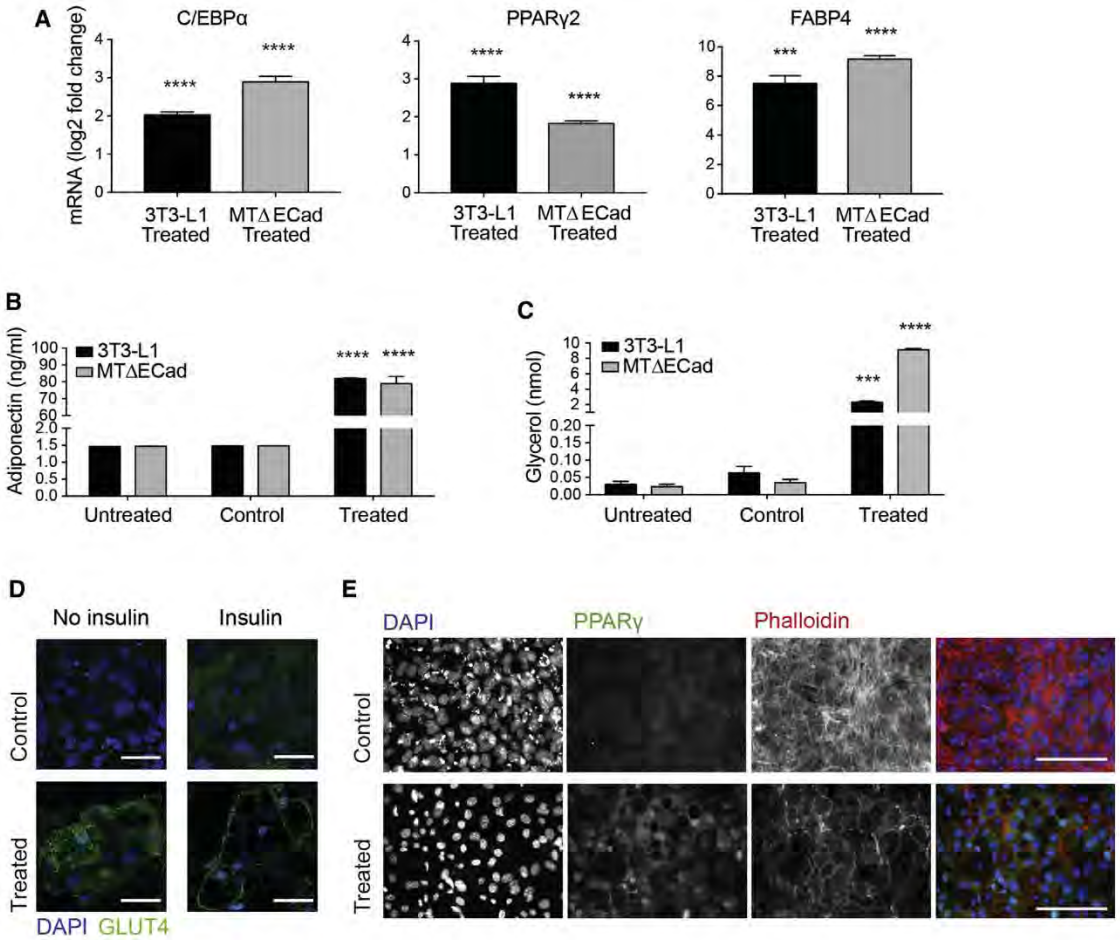

Figure 2. EMT-Derived Breast Cancer Cells Undergo Trans-differentiation into Functional Adipocytes

(A) Fibroblastic pre-adipocytes (3T3-L1) were treated for 10 days with insulin, dexamethasone, and Rosiglitazone to induce adipogenesis. MTΔEcad cells were treated for 10 days with BMP2 and Rosiglitazone. Control cells were treated with DMSO for 10 days. Untreated cells were extracted 24 hr after seeding with growth medium.

Log2-fold change of mRNA levels of the adipocyte-specific regulators PPARγ2 and C/EBPα and the mature adipocyte marker FABP4 compared with control were determined by qRT-PCR in treated cells as indicated. Graphs show means ± SEM (n = 3); unpaired Student's t test.

(B) Adiponectin secretion levels were measured for untreated, control, and treated cells from (A) by ELISA. Ten-day treated cells were compared with control. Graphs show means ± SEM (n = 3); unpaired Student's t test.

(C) Isoproterenol-induced lipolysis was measured in untreated, control, and treated cells from (A). A colorimetric analysis was used to determine glycerol release (lipolysis). Ten-day treated cells were compared with control. Graphs show means ± SEM (n = 3); unpaired Student's t test.

(D) Control and treated MTΔECad cells from (A) were stimulated with insulin for 25 min to induce GLUT4 translocation to the plasma membrane. GLUT4 (green) and DAPI (blue) were visualized by immunofluorescence staining and confocal microscopy. Scale bars, 100 μm.

(E) The adipogenesis regulator PPARγ (green), Phalloidin (F-actin, red), and nuclei (DAPI, blue) were visualized in control and treated MTΔECad cells from (A) by immunofluorescence staining. Scale bars, 100 μm.

***p < 0.0002, ****p < 0.0001. See also Figure S2.

Red staining showed that differentiated MTΔECad and 3T3-L1 cells did not revert to an epithelial or mesenchymal state and maintained their adipocyte characteristics (Figure S2C).

The efficient conversion of MTΔECad murine breast cancer cells into adipocytes *in vitro* allowed a whole transcriptomic survey of gene expression during trans-differentiation into terminally differentiated adipocytes by RNA sequencing. The changes in gene expression during cancer cell adipogenesis were then compared with previously published RNA sequencing data of 3T3-L1 adipogenesis (Al Adhami et al., 2015; GSE50612). Unsupervised clustering revealed a close resemblance of the differentiated states in MTΔECad cancer cell adipogenesis (days 5, 7, and 10) with differentiated 3T3-L1 cells (Figure 3A). Of note, although both differentiation processes were initiated from proliferative mesenchymal cells, the unsupervised clustering underscores the difference between benign (3T3-L1) fibroblasts and malignant (MTΔECad) mesenchymal cells before the induction of adipogenesis (Figure 3A). A clustered heatmap of the most variable genes during the time course of trans-differentiation demonstrated the extensive molecular changes occurring in the cancer cells during forced adipogenesis (Figure 3B). As expected, adipogenesis-related genes were specifically found upregulated in their

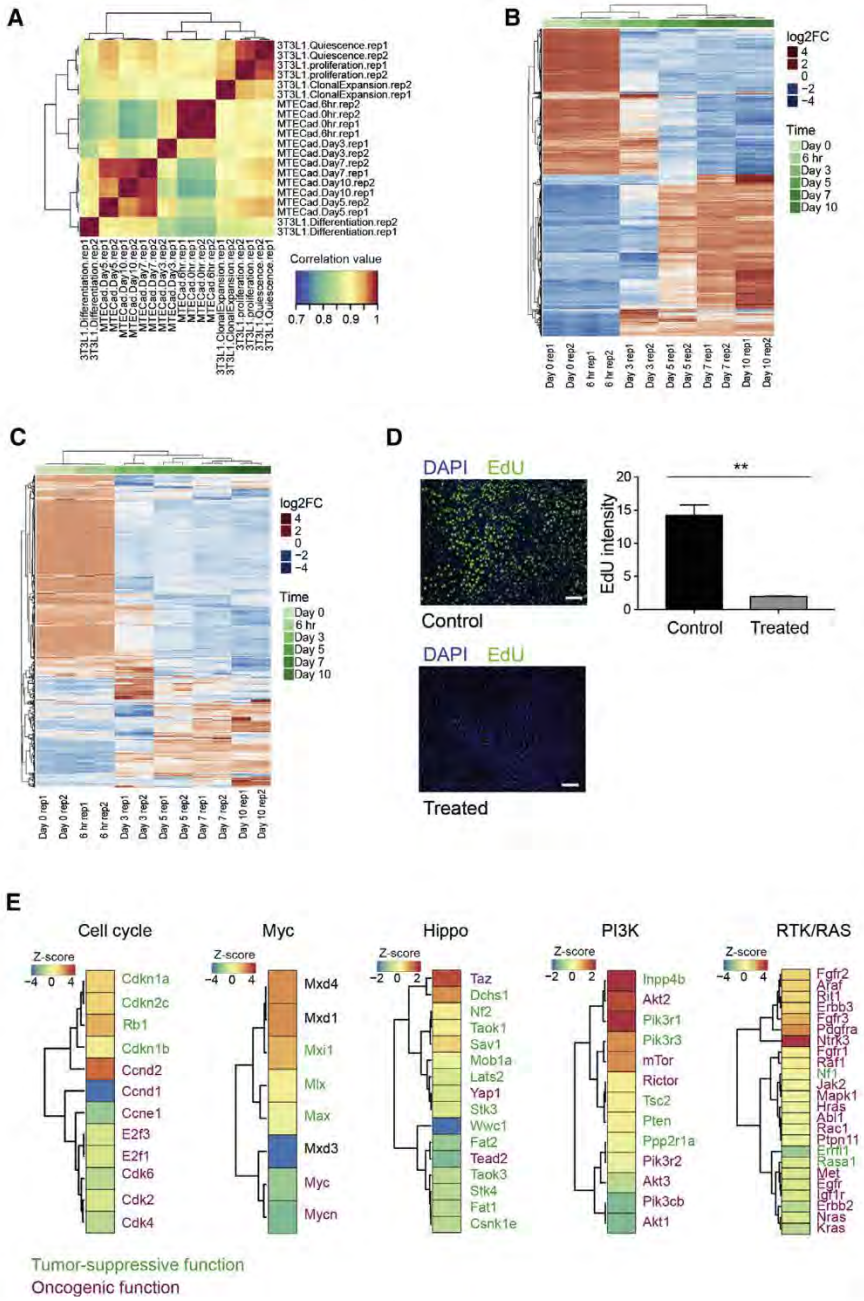

Figure 3. Breast Cancer Cells Undergo bona fide Adipogenesis and Become Post-mitotic

(A) Heatmap comparing gene expression changes in MTΔECad and 3T3-L1 cells undergoing forced adipogenesis *in vitro*. MTΔECad cells were induced to undergo adipogenesis and RNA was extracted for RNA sequencing at the time points indicated in Figure 1C. RNA sequencing data of 3T3-L1 cells undergoing adipogenesis at exponential proliferation, quiescence (48 hr confluence), and differentiation (6 days after addition of IDX [insulin, dexamethasone, and isobutylmethylxanthine] addition). Rep1 and rep2 correspond to biological replicates 1 and 2 (GSE50612). An unsupervised hierarchical heatmap represents the correlation between the two adipogenesis time course data.

(B) Heatmap of the top 25% most variably expressed genes during MTΔECad cell adipogenesis.

(C) Heatmap of cell-cycle-related genes during MTΔECad cell adipogenesis annotated in the Gene Ontology (GO) database (GO: 0007049).

(D) Control and adipogenesis-treated MTΔECad cells were incubated with 5-ethynyl-2′-deoxyuridine (EdU) for 72 hr to label proliferating cells. Representative images of EdU (green) and DAPI (blue) staining are shown. EdU intensities were quantified using ImageJ. The graphs show means ± SEM (n = 3); unpaired Student's t test; $^{**}p < 0.001$. Scale bars, 100 μm.

(E) Log2-fold change of significantly regulated oncogenes and tumor suppressors in different oncogenic pathways (Cell cycle, Myc, Hippo, PI3K, and RTK/RAS) in MTΔECad adipocytes (day 10) versus MTΔECad mesenchymal cells (day 0) are represented as a heatmap. Genes labeled in green are tumor suppressors and those in red are oncogenes.

See also Figure S3.

expression (Figure S3A). Notably, the comparative gene expression analysis identified the differentiated cells as white adipocytes expressing Resistin (*Retn*) and not UCP1 (*Ucp1*), a marker for brown adipocytes (Figure S3B). On the other hand, the expression of genes related to EMT, cell invasion, and extracellular matrix remodeling was found reduced during adipogenic trans-differentiation (Figures S3C and S3D). Yet, the expression of the EMT-related transcription factors Zeb1 and Zeb2 was found enhanced, consistent with their essential functions in adipogenesis (Gubelmann et al., 2014).

As mentioned above, when considering cancer therapy, one of the most appealing characteristics of adipocytes is their cell-cycle arrest. A clustered heatmap of the expression of cell-cycle-related genes during the process of trans-differentiation demonstrated an extensive shift in cell-cycle regulation (Figure 3C). Analysis of specific cell-cycle-related genes showed the downregulation of genes known to induce proliferation alongside with the upregulation of genes known to arrest cell cycle (Figure S3E). Indeed, 5-ethynyl-2′-deoxyuridine incorporation assays revealed an almost complete loss of proliferation of MTΔECad cells forced to trans-differentiate into adipocytes (Figure 3D).

The observations regarding cell-cycle arrest in cancer-derived adipocytes motivated a detailed analysis of oncogenic pathway activation during cancer adipogenesis (Sanchez-Vega et al., 2018). Oncogenic pathways involved in the regulation of cell cycle, Myc transcriptional activity, and receptor tyrosine kinase/RAS signaling showed decreased expression of oncogenic and increased expression of tumor-suppressive genes in cancer-derived adipocytes (Figure 3E). However, some oncogenic pathways are not exclusively connected to cancer cell proliferation. For example mammalian target of rapamycin (mTOR), the

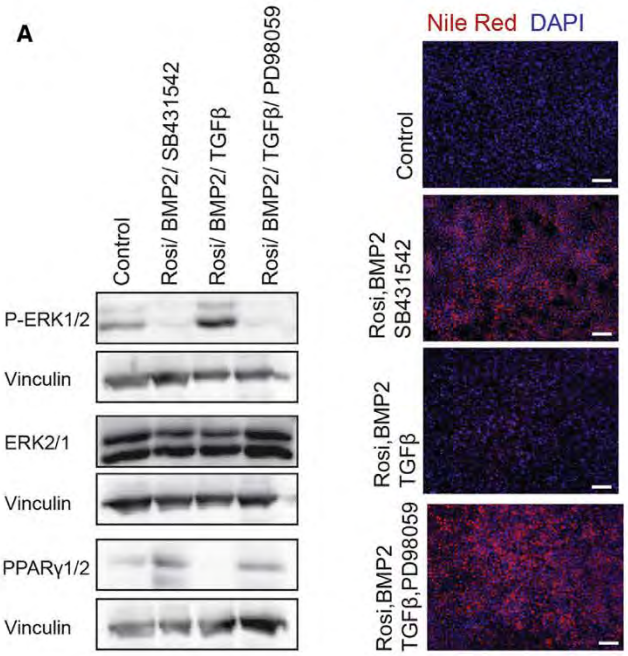

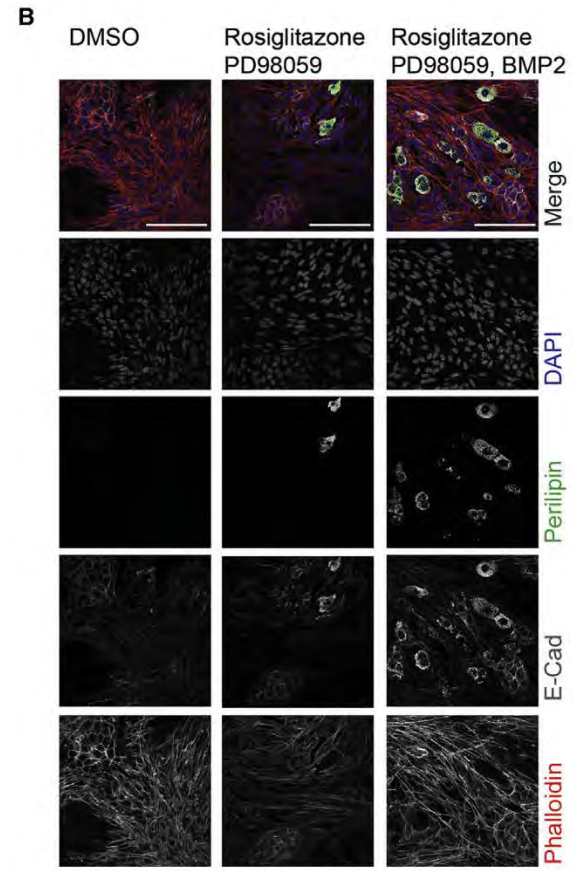

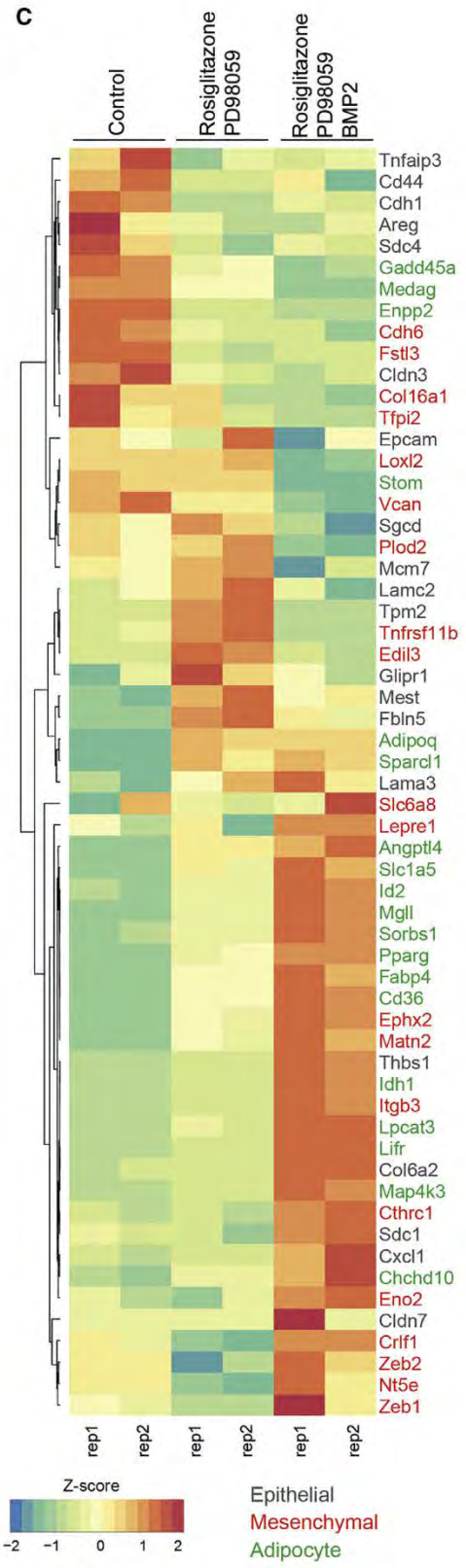

(legend on next page)

downstream effector of the PI3K pathway, exerts a critical role in adipogenesis and adipocyte function (Laplante and Sabatini, 2012). Indeed, the expression of some oncogenes, such as *Akt1*, was found downregulated by adipogenesis, whereas *Mtor* expression was enhanced (Figure 3E). The tumor-suppressive Hippo pathway was generally downregulated during cancer adipogenesis (Figure 3E), and the inhibition of proliferation was contemporaneous with a nuclear to cytoplasmic shift in the subcellular localization of oncogenic Yap (Figures S3F and S3G).

Together, the data demonstrate that mammary gland cancer cells undergoing EMT gain the potential to irreversibly differentiate into bona fide adipocytes with post-mitotic cell-cycle arrest. Epithelial cancer cells lack this potential, supporting the notion that an EMT coincides with increased cell plasticity.

EMT and TGF-β Signaling Regulate Cancer Cell Adipogenesis

Based on the dramatic reprogramming of cells undergoing an EMT, we asked which transcription factors were activated during EMT and were permissive for adipogenesis regulation. RNA sequencing data of a time course of MTΔECad cell adipogenesis was used to predict transcription factor activity by Integrated System for Motif Activity Response Analysis (Balwierz et al., 2014). As expected, regulators of adipogenesis, such as CEBPβ and PPARγ, were detected with increased transcriptional activity during cancer cell adipogenesis (Figure S4A). Zeb1 activity was found increased as well (Figure S4A). In contrast, Klf4 activity negatively correlated with its target gene expression, suggesting that Klf4 acted as a repressor during cancer cell adipogenesis (Figure S4A). As demonstrated for non-cancer adipogenesis (Birsoy et al., 2008; Gubelmann et al., 2014), the downregulation of Zeb1 and Klf4 interfered with cancer adipogenesis, as siRNA-mediated ablation of Zeb1, Zeb2, and Klf4 in the MTΔECad and the Py2T-LT murine mammary gland tumor cells significantly repressed the expression of adipocytic genes (Figures S4B and S4C). Of note, Snail1 expression was found downregulated during cancer adipogenesis (Figure S3D) and its activity reduced (Figure S4A). Indeed, siRNA-mediated knockdown of Snail1 expression promoted adipogenic gene expression (Figure S4B). These data suggest that the transcriptional regulation of EMT and MET are directly connected to the adipogenesis potential of cancer cells.

An important role in EMT/MET regulation is exerted by TGF-β family members. BMPs play a major role in inducing adipogenesis and also are inducers of MET (Samavarchi-Tehrani et al., 2010; Suenaga et al., 2013). On the other hand, TGF-β acts as an inhibitor of adipogenesis, yet is one of the most potent inducers of an EMT, and TGF-β-signaling pathways are activated in metastatic cancer cells (Bruna et al., 2012; Oshimori et al., 2015). The canonical TGF-β-mediator Smad3 appeared highly active in the mesenchymal MTΔECad cells, even after BMP2 induction. However, once cells entered adipogenesis, Smad3 activity was reduced (Figure S4A). To overcome TGF-β-mediated inhibition of adipogenesis, we interrogated which of the TGF-β-induced pathways remained active in the presence of both TGF-β and adipogenesis inducers. As expected, the presence of TGF-β repressed adipogenesis of MTΔECad cells, while the inhibition of TGF-β signaling with the pharmacological inhibitor SB431542 promoted their adipogenesis (Figure 4A). More detailed analysis indicated an activation of non-canonical MEK/ERK pathways in this context (Figure S4D). ERK has been previously reported to interfere with PPARγ function leading to obesity-linked insulin resistance (Banks et al., 2015). Indeed, pharmacological inhibition of MEK/ERK activation with the MEK inhibitor (MEKi) PD98059 allowed the differentiation of mesenchymal cancer cells even in the presence of TGF-β (Figure 4A). We noted that BMP2 had a positive effect on the efficiency of adipogenesis in MTΔECad-irreversible EMT cells, yet to a lesser extent in Py2T-LT-reversible EMT cells (Figure S4E). Instead, in the absence of TGF-β, Py2T-LT cells merely require Rosiglitazone and MEK inhibition for adipocyte differentiation (Figures 4B and S4E). Analysis of gene expression by RNA sequencing revealed that, in Py2T-LT cells, adipogenesis efficiently progressed alongside a mixed epithelial/mesenchymal gene expression pattern, once non-canonical TGF-β signaling was inhibited by the MEKi PD98059, as manifested by the simultaneous expression of the epithelial marker E-cadherin and its mesenchymal transcriptional repressors Zeb1 and 2 (Figures 4B and 4C). These results suggest that adipogenic trans-differentiation of cancer cells might be more efficient when originating from cells in a state of partial/intermediate EMT. We further assessed which cellular mechanisms enhanced the cancer cells' trans-differentiation potential by analyzing the effect of BMP2 on cancer cell adipogenesis. Interestingly, the positive effect of BMP2 on adipogenesis efficiency was directly connected to cell-cycle regulation in both cellular EMT models (Figures S4F–S4I).

The results identify MEK as a potential gatekeeper for the enforcement of EMT-induced cancer cell adipogenesis, consistent with a previous report that MEK inhibitors potentiate normal adipocyte function (Banks et al., 2015). On the other hand, by inducing an EMT, TGF-β increases cancer cell plasticity, but simultaneously inhibits adipogenesis by its non-canonical MEK-ERK pathway. Hence, inhibition of TGF-β-induced

Figure 4. Active TGF-β Signaling in Cancer Cells Requires the Inhibition of the MEK-ERK Pathway to Allow Adipogenesis

(A) MTΔECad cells were treated with DMSO (control), Rosiglitazone (Rosi), BMP2, TGF-β receptor inhibitor (SB431542), TGF-β, and an MEK inhibitor (PD98059) as indicated. After 7 days of treatment, the levels of phosphorylated ERK1/2 (P-ERK1/2) and total ERK (ERK1/2), PPARγ1/2 as an adipogenesis marker and vinculin as loading control were determined by immunoblotting analysis (left panel). After 10 days of treatment, lipid droplets and nuclei were visualized by immunofluorescence staining with Nile Red dye (red) and DAPI (blue) (right panel). Scale bars, 100 μm.

(B) Mesenchymal/epithelial/adipocyte subpopulations in Py2T-LT-treated cells. Py2T-LT cells were treated with Rosiglitazone, PD98059 plus/minus BMP2, or DMSO (control) for 10 days. Immunostaining for adipocyte protein (Perilipin, green), epithelial protein (E-cadherin, E-Cad, gray), and the actin cytoskeleton (Phalloidin, red) were visualized by confocal microscopy. Scale bars, 100 μm.

(C) Mesenchymal-specific (red), epithelial-specific (gray), and adipocyte-specific (green) gene expression in Py2T-LT cells treated as in (B) for 7 days. The heatmap representing the epithelial/mesenchymal/adipocyte markers reveals gene expression similarities and variabilities across the different treatments is constructed using normalized CPM (counts per million) data.

See also Figure S4.

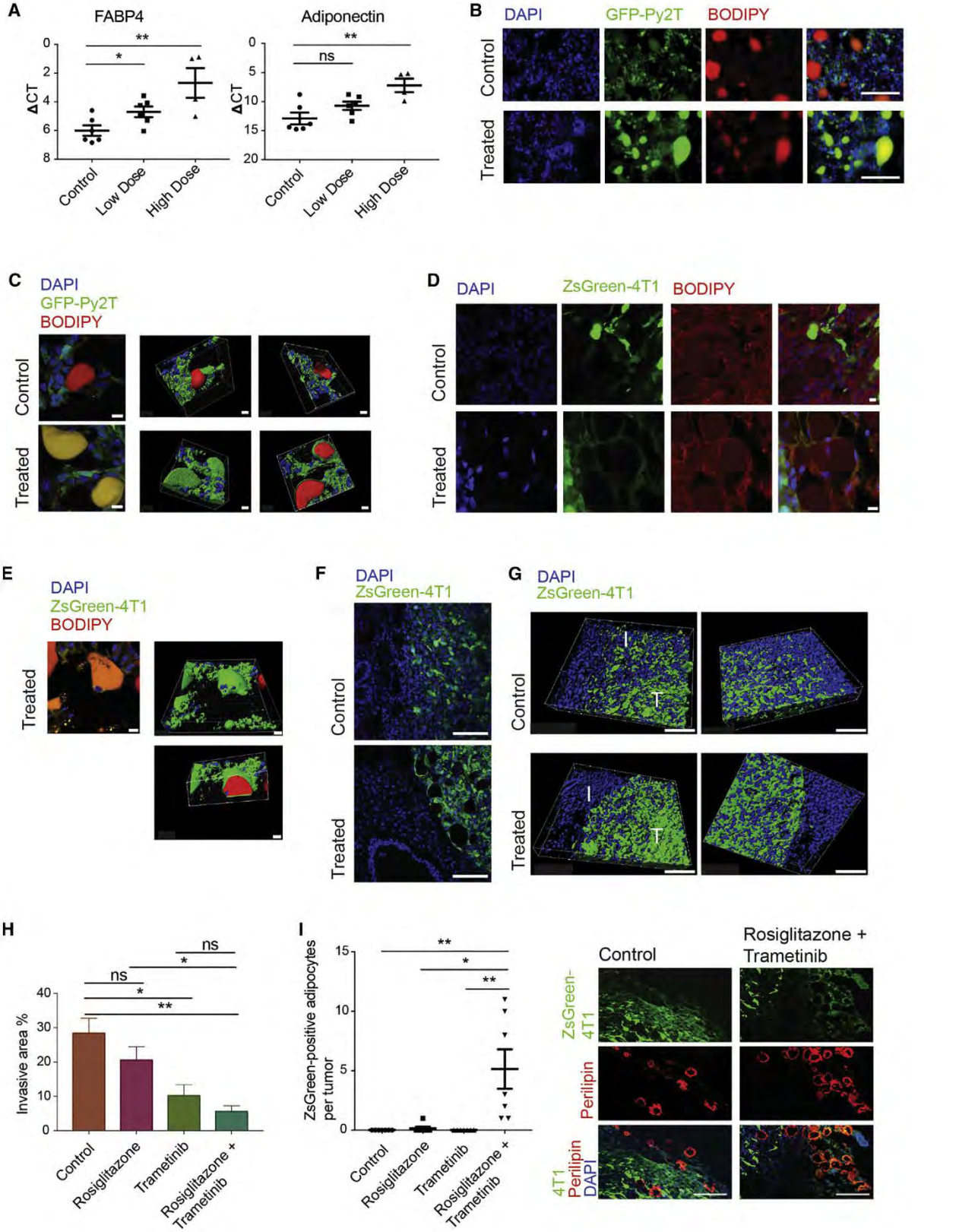

(legend on next page)

MEK-ERK signaling enables an efficient adipogenesis of EMT-derived cancer cells.

Direct Conversion of Tumor Cells into Adipocytes *In Vivo*

The knowledge of how to overcome TGF-β-mediated inhibition of adipogenesis by an MEK inhibitor motivated us to test whether it is possible to differentiate invasive, mesenchymal breast cancer cells into adipocytes in mouse models *in vivo*. In a proof-of-concept study, we evaluated the *in vivo* adipogenesis potential of transplanted GFP-expressing Py2T cells upon treatment with a high or low dose of MEKi PD98059 in combination with Rosiglitazone. While no significant change in tumor growth between the treatment groups was observed (Figure S5A), and body weights were not significantly affected (Figure S5B), the high-dose treatment had a toxic effect on the general well-being of the animals, and the experiment was terminated. Yet, a significantly increased expression of the adipocyte markers FABP4 and adiponectin was detected in the tumors of high-dose Rosiglitazone/MEKi-treated mice and to a lesser extent in the low-dose treatment group (Figure 5A).

We next assessed whether the upregulation of adipocyte markers was due to generally increased adipogenesis in the tumor stroma or due to the cancer cells' direct trans-differentiation into adipocytes. White fat adipocytes exhibit typical adipocyte morphology with a large unilocular lipid droplet (Gesta et al., 2007; Rosen and Spiegelman, 2014). Lipid droplets within cells of tumor sections were visualized by staining with BODIPY, and tumor cells were identified by their GFP expression. Indeed, trans-differentiated tumor cells expressing GFP and containing unilocular lipid droplets were identified in the tumors of Rosiglitazone/MEKi-treated mice and not in the control mice (Figures 5B and 5C).

As a further proof-of-concept experiment, mice transplanted with 4T1 metastatic murine breast cancer cells expressing ZsGreen fluorescent protein were treated with the low-dose combination treatment. Here, body weight and animal health were maintained in both groups (Figure S5C). Although tumor volume was not significantly affected by the treatment (Figure S5D), total tumor mass was found reduced in the combination treatment group (Figure S5E). Tumors of mice treated with MEKi and Rosiglitazone, but not tumors of control-treated mice, exhibited BODIPY-positive adipocytes expressing ZsGreen (Figures 5D and 5E). Notably, ZsGreen-expressing adipocytes predominantly localized at the rim of the tumor next to the normal mammary fat pad. Confocal microscopy and 3D reconstruction analysis of the tumor rims revealed that the highly invasive tumor fronts observed in the control-treated tumors were absent in tumors of Rosiglitazone/MEKi-treated mice (Figures 5F and 5G).

The invasive front of the tumor is suspected to be the main location of invasive cancer cells with increased cell plasticity (Oshimori et al., 2015). We thus hypothesized that targeting these invasive cancer cells with adipogenic trans-differentiation therapy should inhibit tumor invasion. To test this assumption, we employed a combination therapy with the US Food and Drug Administration (FDA)-approved MEK inhibitor Trametinib and with Rosiglitazone in pre-clinically relevant settings. Trametinib demonstrated an efficient inhibition of ERK phosphorylation

Figure 5. Adipogenesis of Breast Cancer Cells *In Vivo*

(A) GFP-expressing Py2T cells were injected into the mammary fat pad of female RSG mice. After initial tumor growth, mice were randomized into three cohorts treated daily with either vehicle (Control), 2 mg/kg MEK inhibitor (PD98059) and 16 mg/kg Rosiglitazone (Low Dose), or 5 mg/kg PD98059 and 16 mg/kg Rosiglitazone (High Dose). After 14 days of treatment mice were sacrificed and tumors analyzed. n = 4–7 mice per group. mRNA levels of FABP4 and adiponectin in tumors were determined by qRT-PCR. The graphs show means ± SEM. Unpaired Student's t test; *p < 0.0332, **p < 0.0021; ns, not significant.

(B) Representative images of adipocytes inside tumors in both control and low combination-treated mice from (A). Tumor cells and lipid droplets were visualized by GFP expression (green) and staining with BODIPY (red), respectively, and fluorescence microscopy. Scale bars, 100 μm.

(C) Co-localization of GFP (labeled Py2T cells) and BODIPY was visualized by confocal microscopy (left side) in Control and Low Dose adipogenesis-treated tumors from (A). The confocal images shown in the middle were reconstructed in 3D using Imaris software allowing optical sectioning of the GFP-positive cells that contain a BODIPY-stained lipid droplet (panels on the right side). Scale bars, 10 μm.

(D) ZsGreen-expressing 4T1 cells were injected into the mammary fat pad of female NMRI nu/nu mice. After initial primary tumor growth, mice were treated daily with vehicle (Control) or with 2 mg/kg MEKi PD98059 and 16 mg/kg Rosiglitazone (Treated). After 17 days of treatment, mice were euthanized and tumors analyzed. n = 6 mice per group. Representative images of adipocytes inside tumors in both control and treated mice are shown. Lipid droplets were visualized with BODIPY (red), tumor cells were visualized by ZsGreen, and nuclei by DAPI staining and confocal microscopy on 80-μm-thick frozen sections. Scale bars, 10 μm.

(E) Treated tumor sections from (D) were stained with BODIPY (red) to identify adipocyte structures formed by differentiated 4T1 cells (green) using confocal microscopy (left image). 3D reconstruction and optical sectioning of the confocal microscopy images using Imaris software (right images). Scale bars, 10 μm.

(F) Representative confocal microscopy images of the invasive front in control and adipogenesis-treated tumors from (D). Tumor cells were visualized by ZsGreen (green) and nuclei by DAPI (blue) staining. Scale bars, 100 μm.

(G) Frozen sections (80-μm-thick) of tumor rims from (D) were analyzed by confocal microscopy and visualized by 3D reconstructions using Imaris software. Scale bars, 100 μm. Tumor bulk (T) and the invasive area/border (I) are labeled.

(H) ZsGreen-expressing 4T1 murine breast cancer cells were injected into the mammary fat pad of female NMRI nu/nu mice. After initial primary tumor growth, mice were treated daily with vehicle (Control), Rosiglitazone (20 mg/kg) alone, Trametinib (0.3 mg/kg) alone, or with a combination of Rosiglitazone (20 mg/kg) and Trametinib (0.3 mg/kg). After 17 days of treatment, mice were euthanized, and tumors and lungs were processed for histopathological analysis (n = 7 mice per group). Primary tumor invasion at the tumor rim was quantified by defining the tumor borders to the surrounding tissues in complete section images as shown in (Figure S5J) and determining the percentage of GFP-positive cells at the invasive front.

(I) Perilipin immunostaining was used to visualize lipid droplet membranes within tumor frozen sections from (H). Complete section imaging was preformed using a confocal spinning disc microscope. ZsGreen staining identified tumor cells, and double-positive cells at the tumor invasive fronts were quantified as tumor cells that have undergone adipogenesis *in vivo* (ZsGreen-adipocytes). Representative images from control and Rosiglitazone + Trametinib treated groups are shown. Scale bars, 200 μm. The graphs in (H and I) show means ± SEM; Kruskal-Wallis test corrected for multiple comparisons. *p < 0.0332, **p < 0.0021; ns, not significant.

See also Figure S5.

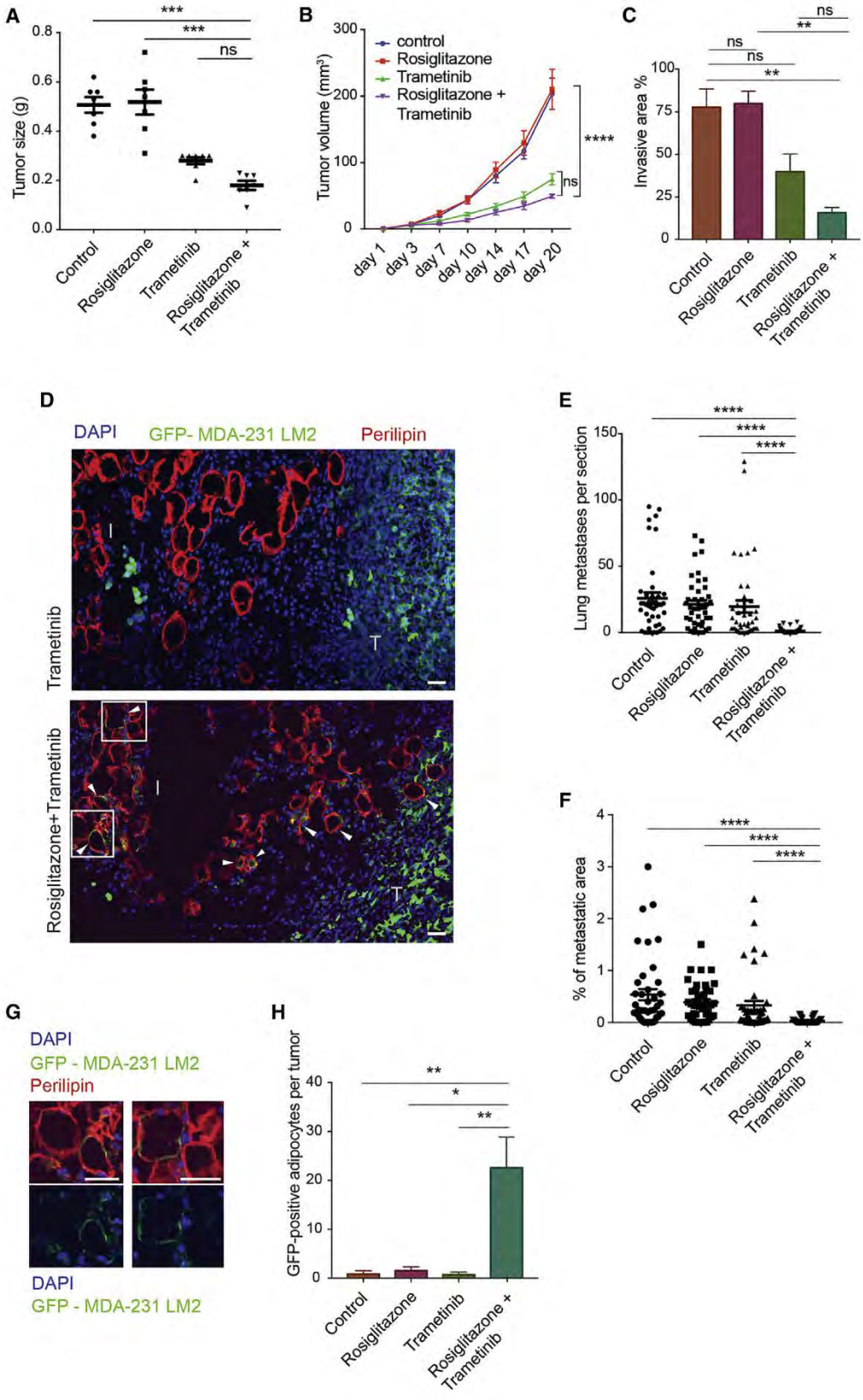

(legend on next page)

and induction of adipocyte differentiation in cultured MTΔECad cells (Figure S5F). We then tested whether combination of Rosiglitazone with Trametinib showed an induction of adipogenesis and repression of invasiveness comparable with combination with PD98059 in mice transplanted with ZsGreen-expressing 4T1 tumors. The treatment exerted no toxic effects as evaluated by animal appearance and body weight (Figure S5G). The repression of primary tumor growth and tumor mass by Trametinib alone was already substantial and showed no additional significant effect by the combination with Rosiglitazone (Figures S5H and S5I). To assess the extent of adipogenesis and potential effects on tumor invasion in these experimental settings, histological sections of 4T1 tumors were stained with Perilipin, the most abundant protein on the surface of lipid droplets in white and brown adipocytes (Brasaemle, 2007). Quantification of the invasive versus non-invasive fronts at the tumor borders showed a significant reduction of tumor invasion in the Trametinib only- and combination-treated groups (Figures 5H and S5J). Moreover, ZsGreen-positive adipocytes were found significantly increased only in the tumors of the combination treatment group, mainly at the rim of the tumors (Figure 5I).

Adipogenesis Therapy Represses Invasion and Metastasis Formation

We next assessed whether the adipogenic trans-differentiation therapy of invasive cancer cells would also repress metastatic seeding and outgrowth. Mice implanted with GFP-expressing MDA-MB 231 LM2 human breast cancer cells, known to preferentially metastasize to the lungs (Minn et al., 2005), were treated with solvent as control, Rosiglitazone only, Trametinib only, or a combination thereof. The treatments did not elicit any apparent toxic effects or body weight changes (Figure S6A). Tumor growth was found impeded in the Trametinib and combination treatment groups, yet the repression of primary tumor growth by Trametinib alone was not significantly increased by the combination treatment (Figures 6A and 6B). Tumor vascularization (Figure S6B) as well as cancer cell proliferation and apoptosis (data not shown) were not significantly affected. Perilipin staining to visualize adipocyte-specific lipid droplets showed a slight, but not significant reduction of tumor invasion in the Trametinib only-treated group, while tumor invasion was significantly repressed by the combination of Trametinib with Rosiglitazone (Figures 6C, 6D, and S6C).

Quantification of the number and relative area of lung metastases in histological lung sections of mice transplanted with MDA-MB 231 LM2 and treated with the four different regimens described above demonstrated an almost complete abrogation of metastasis formation in the Trametinib/Rosiglitazone combination group as compared with the control groups (Figures 6E and 6F). A Spearman correlation between the extent of primary tumor invasiveness and metastatic incidence was found highly significant (Figure S6D), suggesting that the lack of local tumor invasion by the combination treatment caused a substantial repression of metastasis formation. Notably, when analyzing tumor sections of the various treatment groups we observed that, upon combination treatment, the highly mesenchymal MDA-MB 231 LM2 tumors exhibited a rather benign, in parts differentiated morphology. Indeed, immunoblotting analysis revealed a significant upregulation of E-cadherin expression in the Trametinib and in particular in the Rosiglitazone/Trametinib treatment group (Figure S6E). GFP and Perilipin double-positive, cancer cell-derived adipocytes were found exclusively within the tumor bulk (Figure S6F) and tumor rims of mice treated with the combination of Trametinib and Rosiglitazone (Figures 6D, 6G, and 6H).

Together, the data demonstrate that the combination treatment with Trametinib and Rosiglitazone targets invasive cancer cells and prevents metastasis formation by forcing invasive cancer cells into adipogenesis.

Adipogenesis Therapy in a Preclinical Patient-Relevant Setting

To test the long-term effect of adipogenesis therapy in an experimental design closely recapitulating the clinical situation with breast cancer patients, we used a patient-derived xenograft (PDX) model of human breast cancer in a preclinical, neoadjuvant setting. PDX models of human cancers were previously established and characterized to allow preclinical evaluation of treatment modalities (Byrne et al., 2017). The PDX model (number x-3078) used here has been previously established from a treatment-naive primary tumor and characterized as a triple-negative breast cancer (with 2% ER^+ cells as determined by

Figure 6. Adipogenesis Therapy Represses Primary Tumor Invasion and Lung Metastasis of MDA-MB 231 LM2 Human Breast Cancer Cells

(A) GFP-expressing MDA-MB 231 LM2 human cells were injected into the mammary fat pad of female NSG mice. After initial primary tumor growth, mice were treated daily with vehicle (Control), with Rosiglitazone (20 mg/kg), with Trametinib (0.3 mg/kg), or with a combination of Rosiglitazone (20 mg/kg) and Trametinib (0.3 mg/kg). After 3 weeks of treatment, mice were euthanized, and tumors and lungs were processed for histopathological analysis (n = 7 mice per group). Tumor mass was determined after euthanasia.

(B) Tumor volume growth curves from (A) are shown during treatment time course. Significance calculation of linear regression between the groups was calculated based on mean-t statistic and p value adjustment as described by Holm-Bonferroni method.

(C and D) Primary tumor invasion at the tumor rim was quantified for tumors (C) of the four treatment cohorts in (A). For the analysis, tumor borders to the surrounding tissues in complete section images as shown in (D) were defined, and the percentage of the invasive area was determined. (D) Representative images of tumor sections from (A) stained with DAPI and Perilipin. Complete section imaging was performed using a confocal spinning disc microscope. Tumor fronts at the rim of the tumor (T) and the surrounding stroma (I) are shown. Arrowheads indicate GFP-positive (tumor cells) adipocytes. Magnification boxes of Perilipin-positive cells are shown in (G). Scale bars, 50 μm.

(E and F) Lung sections (six sections per mouse) from (A) were stained with H&E and imaged using an Axio Imager scanning microscope (Zeiss). The number of lung metastasis per section (E) and the percentage of metastatic area per lung section (F) were quantified using VIS software.

(G) Magnification of the boxes indicated in the lower image of (D) showing GFP-positive (tumor-derived) and GFP-negative (stroma-derived) Perilipin-positive adipocytes. Scale bars, 50 μm.

(H) GFP-positive adipocytes, as shown in (D and G) were quantified.

Graphs shows means ± SEM. Kruskal-Wallis test corrected for multiple comparisons unless otherwise indicated.

*p < 0.0332, **p < 0.0021, ***p < 0.0002, ****p < 0.0001; ns, not significant. See also Figure S6.

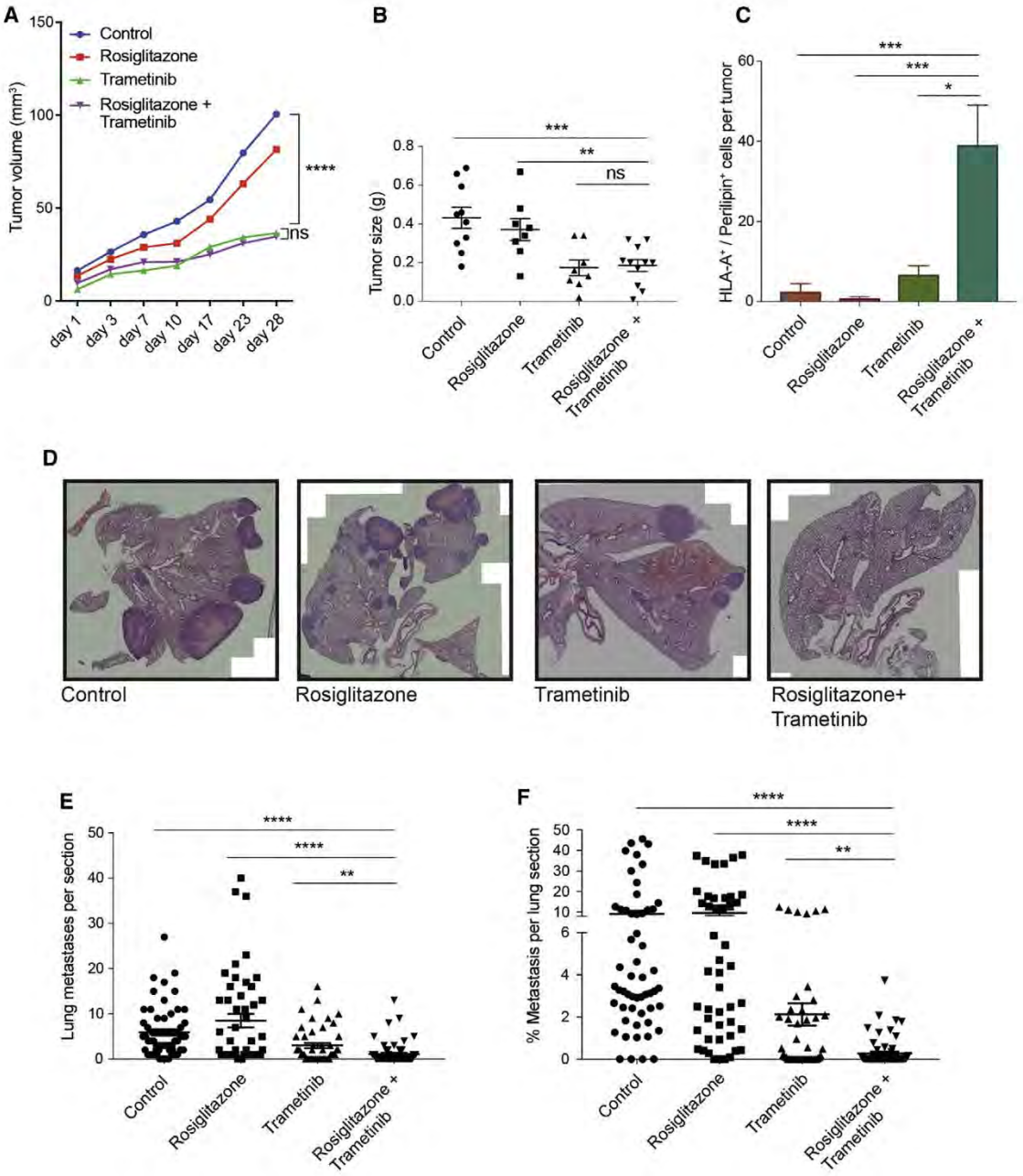

Figure 7. Adipogenesis Therapy Represses Metastasis Formation in a Clinically Relevant Setting with a PDX Human Breast Cancer Model

(A) Patient-derived human breast cancer tumor pieces were transplanted into the mammary fat pad of female NSG mice. Four weeks post-transplantation, mice were treated daily with vehicle (Control), Rosiglitazone (20 mg/kg) alone, Trametinib (0.3 mg/kg) alone, or a combination of Rosiglitazone (20 mg/kg) and Trametinib (0.3 mg/kg). Eight weeks post-transplantation tumors were surgically removed, and mice were treated for further 8 weeks. Mice were then euthanized, and lungs were processed for histopathological analysis. n = 8–11 mice per treatment group. Tumor volume growth curves are shown during treatment until primary tumor removal. Significance calculation of linear regression between the groups was calculated based on mean-t statistic and p value adjustment as described by Holm-Bonferroni method.

(B) Tumor mass after surgical removal of the primary tumor in (A).

(C) Tumor sections from (A) were stained with HLA-A (human cancer cells) and Perilipin (adipocytes) antibodies and DAPI. Complete section imaging was performed using a confocal spinning disc microscope. HLA-expressing adipocytes were quantified.

(D–F) Lung sections (six sections per mouse) from (A) were stained with H&E and imaged using an Axio Imager scanning microscope (Zeiss). Representative images are shown in (D). White boxed areas did not contain tissues and have not been imaged by the automated scanning microscope. The number (E) and relative area (F) of lung metastases per section were quantified using VIS software.

Graphs show means ± SEM. Kruskal-Wallis test corrected for multiple comparisons unless otherwise indicated. *$p < 0.0332$, **$p < 0.0021$, ***$p < 0.0002$, ****$p < 0.0001$; ns, not significant. See also Figure S7.

immunohistochemistry) carrying *PIK3CA*, *BRCA1*, and *TP53* mutations (Gao et al., 2015). After implantation and primary tumor growth for 4 weeks, mice were randomly divided into four groups and treated with vehicle only (Control), Rosiglitazone alone, Trametinib alone, and a combination of Rosiglitazone and Trametinib. Primary tumor growth was monitored (Figure 7A), and 8 weeks post-transplantation primary tumors were surgically removed and tumor mass was determined (Figure 7B). Notably, a reduction of primary tumor growth appears due to Trametinib treatment, since Trametinib alone and the combination therapy comparably repressed primary tumor growth (Figures 7A and 7B). Staining with CD31 antibodies did not reveal any significant changes in tumor vascularization (Figure S7A). After primary tumor removal, mice were kept under therapy and then euthanized 4 months post-transplantation. Body weights were monitored during the experiment with no significant differences between the groups (Figure S7B).

As the primary tumors were surgically removed, the tumor rims were too narrow to allow the quantification of primary tumor invasiveness. The patient-derived human cells were detected by anti-HLA-A staining in a background of host mouse tissue visualized by anti-H2K^d staining. Notably, co-staining of Perilipin together with HLA-A detected human-origin adipocytes with the highest numbers in combination-treated cells (Figures 7C and S7C). Quantification of the number and relative areas of lung metastases demonstrated a significant repression of metastasis formation and metastatic outgrowth in the combination treatment group as compared with the control groups (Figures 7D–7F).

Together, the results indicate that in a patient-relevant setting combined therapy with Rosiglitazone and Trametinib specifically targets cancer cells with increased plasticity and induces their adipogenesis. As a consequence, adipogenesis therapy exerts a long-term inhibition of metastasis initiation and outgrowth by trans-differentiating invasive cancer cells into adipocytes.

DISCUSSION

In this study, we report a therapeutic approach to target cancer cell plasticity by forcing the trans-differentiation of breast cancer cells into bona fide adipocytes.

PPARγ agonists, such as Rosiglitazone, were previously shown to induce cellular re-differentiation in a variety of malignancies (Mueller et al., 1998; Prost et al., 2015; Tontonoz et al., 1997). Yet, in line with our *in vivo* results, Rosiglitazone and other PPARγ ligands alone had a limited benefit treating carcinomas in a clinical setting. Here we demonstrate that Rosiglitazone in combination with MEK inhibitors enhances epithelial differentiation and adipogenesis both *in vitro* and *in vivo*. Thus, it is possible that inhibition of MEK allows the differentiation of cancer cells depending on the activation of a particular differentiation pathway. Adipogenesis induction, predominantly of disseminating cancer cells, may be linked to increased cell plasticity induced by the tumor microenvironment. Indeed, TGF-β is a major contributor to EMT and cancer cell plasticity *in vivo*. However, while TGF-β is a major driver of malignant progression, it affects only few cells in the invasive front of primary tumors (Oshimori et al., 2015). Our results demonstrate that cancer cells that have left the primary tumor site and invaded into the surrounding tissue, i.e., cells that have most likely undergone an EMT, have been directly affected by the therapeutic treatment and have trans-differentiated into post-mitotic adipocytes. As noted, while cancer cell apoptosis does not seem to be affected by the trans-differentiation therapy, cancer cell proliferation is, in that cell-cycle-promoting genes are repressed and cell-cycle inhibitors are induced to convert the cells into post-mitotic adipocytes. In addition, while the mixed expression of mesenchymal and epithelial marker genes in cells receiving adipogenesis therapy indicates a high cell plasticity of a partial or intermediate EMT, the benign histopathology of the treated primary tumors in the different mouse models demonstrates the potential of the therapeutic approach to repress tumor invasion and malignant progression.

The trans- and re-differentiation potential of invasive cancer cells *in vivo* compares to cellular features observed in EMT-induced cells *in vitro*, which represent characteristics of a partial EMT. The transcription factors regulating the adipogenesis potential of cancer cells, such as Zeb1, Zeb2, and Klf4, are linked both to EMT/MET as well as to pluripotency and stemness. Partial EMT has recently been associated with increased intra-tumor plasticity and metastatic potential (Pastushenko et al., 2018). These data indicate that cancer cell plasticity, as for example demarcated by a partial EMT, enhances stem cell-like gene regulation, which in turn enables cancer cell trans-differentiation.

The models used in this study have allowed the evaluation of disseminating cancer cell adipogenesis in the immediate tumor surroundings. The clinical evaluation of the treatment's repressive effect on experimental breast cancer metastasis and, thus, of its potential in treating stage IV breast cancer will require adjuvant combinations with chemotherapy in advanced preclinical models. Since we have used FDA-approved drugs to study the preclinical effect of the treatment, a clinical translation may be possible. Trametinib's effects on different systemic and tumor-specific parameters have been broadly studied. For example, it has been shown that Trametinib has a synergistic effect when combined with immune-modulatory antibodies (Liu et al., 2015), another potential to follow up with the adipogenic trans-differentiation therapy reported here. Finally, since EMT has been demonstrated to increase resistance to chemotherapy and targeted therapy, we envision that the ablation of invasive mesenchymal cancer cells by trans-differentiation therapy may also overcome therapy resistance and cancer relapse.

STAR★METHODS

Detailed methods are provided in the online version of this paper and include the following:

- KEY RESOURCES TABLE
- CONTACT FOR REAGENT AND RESOURCE SHARING
- EXPERIMENTAL MODEL AND SUBJECT DETAILS
  - Cell Lines and Cell Culture
  - Mice
  - Human Material
- METHOD DETAILS
  - In Vitro Adipogenesis
  - In Vitro Chondrogenesis
  - In Vitro Osteogenesis

SUPPLEMENTAL INFORMATION

Supplemental Information includes seven figures and one table and can be found with this article online at https://doi.org/10.1016/j.ccell.2018.12.002.

ACKNOWLEDGMENTS

We thank B. Deplancke (EPFL, Lausanne), N. Aceto, R. Zeller, G. Nusspaumer, and S. Jaiswal (DBM, University of Basel) for reagents and protocols, M. Obradovic and M. Bentires-Alj (DBM, University of Basel) for proving the PDX mice, and M. Saxena (DBM, University of Basel) for advice and discussions. We thank H. Antoniadis and M. Neutzner for technical assistance, E. Fagiani and T. Bürglin for flow cytometry, C. Beisel and the Genomics Facility Basel for next generation RNA sequencing, and P. Lorentz and the microscopy core facility at DBM, University of Basel, for microscopy. Calculations were performed at sciCORE scientific computing core facility at University of Basel (http://scicore.unibas.ch/).

This work was supported by the Botnar Foundation Basel, the SystemsX.ch RTD project Cellplasticity, the SystemsX.ch MTD project MetastasiX, the Swiss National Science Foundation, and the Swiss Cancer League.

AUTHOR CONTRIBUTIONS

D.I.R. designed and performed the experiments, analyzed the data, and wrote the paper. M.D., N.S., S.T., G.B., M.F.M., J.W., and C.H. designed and performed the experiments and analyzed the data. R.I. and R.K.R.K. performed bioinformatics analysis. G.C. oversaw the project, designed experiments, analyzed the data, and wrote the paper.

DECLARATION OF INTERESTS

The authors declare no conflicts of interest.

Received: April 11, 2018
Revised: August 21, 2018
Accepted: December 5, 2018
Published: January 14, 2019

REFERENCES

Al Adhami, H., Evano, B., Le Digarcher, A., Gueydan, C., Dubois, E., Parrinello, H., Dantec, C., Bouschet, T., Varrault, A., and Journot, L. (2015). A systems-level approach to parental genomic imprinting: the imprinted gene network includes extracellular matrix genes and regulates cell cycle exit and differentiation. Genome Res. *25*, 353–367.

Balwierz, P.J., Pachkov, M., Arnold, P., Gruber, A.J., Zavolan, M., and van Nimwegen, E. (2014). ISMARA: automated modeling of genomic signals as a democracy of regulatory motifs. Genome Res. *24*, 869–884.

Banks, A.S., McAllister, F.E., Camporez, J.P., Zushin, P.J., Jurczak, M.J., Laznik-Bogoslavski, D., Shulman, G.I., Gygi, S.P., and Spiegelman, B.M. (2015). An ERK/Cdk5 axis controls the diabetogenic actions of PPARgamma. Nature *517*, 391–395.

Battula, V.L., Evans, K.W., Hollier, B.G., Shi, Y., Marini, F.C., Ayyanan, A., Wang, R.Y., Brisken, C., Guerra, R., Andreeff, M., et al. (2010). Epithelial-mesenchymal transition-derived cells exhibit multilineage differentiation potential similar to mesenchymal stem cells. Stem Cells *28*, 1435–1445.

Birsoy, K., Chen, Z., and Friedman, J. (2008). Transcriptional regulation of adipogenesis by KLF4. Cell Metab. *7*, 339–347.

Brabletz, T. (2012a). EMT and MET in metastasis: where are the cancer stem cells? Cancer Cell *22*, 699–701.

Brabletz, T. (2012b). To differentiate or not–routes towards metastasis. Nat. Rev. Cancer *12*, 425–436.

Brabletz, T., Kalluri, R., Nieto, M.A., and Weinberg, R.A. (2018). EMT in cancer. Nat. Rev. Cancer *18*, 128–134.

Brasaemle, D.L. (2007). Thematic review series: adipocyte biology. The perilipin family of structural lipid droplet proteins: stabilization of lipid droplets and control of lipolysis. J. Lipid Res. *48*, 2547–2559.

Bruna, A., Greenwood, W., Le Quesne, J., Teschendorff, A., Miranda-Saavedra, D., Rueda, O.M., Sandoval, J.L., Vidakovic, A.T., Saadi, A., Pharoah, P., et al. (2012). TGFbeta induces the formation of tumour-initiating cells in claudinlow breast cancer. Nat. Commun. *3*, 1055.

Byrne, A.T., Alferez, D.G., Amant, F., Annibali, D., Arribas, J., Biankin, A.V., Bruna, A., Budinska, E., Caldas, C., Chang, D.K., et al. (2017). Interrogating open issues in cancer precision medicine with patient-derived xenografts. Nat. Rev. Cancer *17*, 254–268.

de The, H. (2018). Differentiation therapy revisited. Nat. Rev. Cancer *18*, 117–127.

Diepenbruck, M., Tiede, S., Saxena, M., Ivanek, R., Kalathur, R.K.R., Luond, F., Meyer-Schaller, N., and Christofori, G. (2017). miR-1199-5p and Zeb1 function in a double-negative feedback loop potentially coordinating EMT and tumour metastasis. Nat. Commun. *8*, 1168.

Dobin, A., Davis, C.A., Schlesinger, F., Drenkow, J., Zaleski, C., Jha, S., Batut, P., Chaisson, M., and Gingeras, T.R. (2013). STAR: ultrafast universal RNA-seq aligner. Bioinformatics *29*, 15–21.

Fantozzi, A., Gruber, D.C., Pisarsky, L., Heck, C., Kunita, A., Yilmaz, M., Meyer-Schaller, N., Cornille, K., Hopfer, U., Bentires-Alj, M., et al. (2014). VEGF-mediated angiogenesis links EMT-induced cancer stemness to tumor initiation. Cancer Res. *74*, 1566–1575.

Fischer, K.R., Durrans, A., Lee, S., Sheng, J., Li, F., Wong, S.T., Choi, H., El Rayes, T., Ryu, S., Troeger, J., et al. (2015). Epithelial-to-mesenchymal transition is not required for lung metastasis but contributes to chemoresistance. Nature *527*, 472–476.

Gao, H., Chakraborty, G., Lee-Lim, A.P., Mo, Q., Decker, M., Vonica, A., Shen, R., Brogi, E., Brivanlou, A.H., and Giancotti, F.G. (2012). The BMP inhibitor Coco reactivates breast cancer cells at lung metastatic sites. Cell *150*, 764–779.

Gao, H., Korn, J.M., Ferretti, S., Monahan, J.E., Wang, Y., Singh, M., Zhang, C., Schnell, C., Yang, G., Zhang, Y., et al. (2015). High-throughput screening using patient-derived tumor xenografts to predict clinical trial drug response. Nat. Med. *21*, 1318–1325.

Gesta, S., Tseng, Y.H., and Kahn, C.R. (2007). Developmental origin of fat: tracking obesity to its source. Cell *131*, 242–256.

Girnun, G.D., Naseri, E., Vafai, S.B., Qu, L., Szwaya, J.D., Bronson, R., Alberta, J.A., and Spiegelman, B.M. (2007). Synergy between PPARgamma ligands and platinum-based drugs in cancer. Cancer Cell *11*, 395–406.

Green, H., and Kehinde, O. (1975). An established preadipose cell line and its differentiation in culture. II. Factors affecting the adipose conversion. Cell *5*, 19–27.

Gubelmann, C., Schwalie, P.C., Raghav, S.K., Roder, E., Delessa, T., Kiehlmann, E., Waszak, S.M., Corsinotti, A., Udin, G., Holcombe, W., et al. (2014). Identification of the transcription factor ZEB1 as a central component of the adipogenic gene regulatory network. Elife *3*, e03346.

Gubser, P.M., Bantug, G.R., Razik, L., Fischer, M., Dimeloe, S., Hoenger, G., Durovic, B., Jauch, A., and Hess, C. (2013). Rapid effector function of memory CD8+ T cells requires an immediate-early glycolytic switch. Nat. Immunol. *14*, 1064–1072.

Gupta, P.B., Onder, T.T., Jiang, G., Tao, K., Kuperwasser, C., Weinberg, R.A., and Lander, E.S. (2009). Identification of selective inhibitors of cancer stem cells by high-throughput screening. Cell *138*, 645–659.

Holohan, C., Van Schaeybroeck, S., Longley, D.B., and Johnston, P.G. (2013). Cancer drug resistance: an evolving paradigm. Nat. Rev. Cancer *13*, 714–726.

Hong, J.H., Hwang, E.S., McManus, M.T., Amsterdam, A., Tian, Y., Kalmukova, R., Mueller, E., Benjamin, T., Spiegelman, B.M., Sharp, P.A., et al. (2005). TAZ, a transcriptional modulator of mesenchymal stem cell differentiation. Science *309*, 1074–1078.

Jordan, N.V., Bardia, A., Wittner, B.S., Benes, C., Ligorio, M., Zheng, Y., Yu, M., Sundaresan, T.K., Licausi, J.A., Desai, R., et al. (2016). HER2 expression identifies dynamic functional states within circulating breast cancer cells. Nature *537*, 102–106.

Kim, M.Y., Oskarsson, T., Acharyya, S., Nguyen, D.X., Zhang, X.H., Norton, L., and Massague, J. (2009). Tumor self-seeding by circulating cancer cells. Cell *139*, 1315–1326.

Kopinke, D., Roberson, E.C., and Reiter, J.F. (2017). Ciliary hedgehog signaling restricts injury-induced adipogenesis. Cell *170*, 340–351.e12.

Koren, S., Reavie, L., Couto, J.P., De Silva, D., Stadler, M.B., Roloff, T., Britschgi, A., Eichlisberger, T., Kohler, H., Aina, O., et al. (2015). PIK3CA(H1047R) induces multipotency and multi-lineage mammary tumours. Nature *525*, 114–118.

Krebs, A.M., Mitschke, J., Lasierra Losada, M., Schmalhofer, O., Boerries, M., Busch, H., Boettcher, M., Mougiakakos, D., Reichardt, W., Bronsert, P., et al. (2017). The EMT-activator Zeb1 is a key factor for cell plasticity and promotes metastasis in pancreatic cancer. Nat. Cell Biol. *19*, 518–529.

Laplante, M., and Sabatini, D.M. (2012). mTOR signaling in growth control and disease. Cell *149*, 274–293.

Lawson, D.A., Bhakta, N.R., Kessenbrock, K., Prummel, K.D., Yu, Y., Takai, K., Zhou, A., Eyob, H., Balakrishnan, S., Wang, C.Y., et al. (2015). Single-cell analysis reveals a stem-cell program in human metastatic breast cancer cells. Nature *526*, 131–135.

Lefterova, M.I., Zhang, Y., Steger, D.J., Schupp, M., Schug, J., Cristancho, A., Feng, D., Zhuo, D., Stoeckert, C.J., Jr., Liu, X.S., et al. (2008). PPARgamma and C/EBP factors orchestrate adipocyte biology via adjacent binding on a genome-wide scale. Genes Dev. *22*, 2941–2952.

Lehembre, F., Yilmaz, M., Wicki, A., Schomber, T., Strittmatter, K., Ziegler, D., Kren, A., Went, P., Derksen, P.W., Berns, A., et al. (2008). NCAM-induced focal adhesion assembly: a functional switch upon loss of E-cadherin. EMBO J. *27*, 2603–2615.

Liu, L., Mayes, P.A., Eastman, S., Shi, H., Yadavilli, S., Zhang, T., Yang, J., Seestaller-Wehr, L., Zhang, S.Y., Hopson, C., et al. (2015). The BRAF and MEK inhibitors Dabrafenib and Trametinib: effects on immune function and in combination with immunomodulatory antibodies targeting PD-1, PD-L1, and CTLA-4. Clin. Cancer Res. *21*, 1639–1651.

Massague, J., and Obenauf, A.C. (2016). Metastatic colonization by circulating tumour cells. Nature *529*, 298–306.

Minn, A.J., Gupta, G.P., Siegel, P.M., Bos, P.D., Shu, W., Giri, D.D., Viale, A., Olshen, A.B., Gerald, W.L., and Massague, J. (2005). Genes that mediate breast cancer metastasis to lung. Nature *436*, 518–524.

Mueller, E., Sarraf, P., Tontonoz, P., Evans, R.M., Martin, K.J., Zhang, M., Fletcher, C., Singer, S., and Spiegelman, B.M. (1998). Terminal differentiation of human breast cancer through PPAR gamma. Mol. Cell *1*, 465–470.

Nieto, M.A. (2013). Epithelial plasticity: a common theme in embryonic and cancer cells. Science *342*, 1234850.

Nieto, M.A., Huang, R.Y., Jackson, R.A., and Thiery, J.P. (2016). Emt: 2016. Cell *166*, 21–45.

Nusspaumer, G., Jaiswal, S., Barbero, A., Reinhardt, R., Ishay Ronen, D., Haumer, A., Lufkin, T., Martin, I., and Zeller, R. (2017). Ontogenic identification and analysis of mesenchymal stromal cell populations during mouse limb and long bone development. Stem Cell Reports *9*, 1124–1138.

Ocana, O.H., Corcoles, R., Fabra, A., Moreno-Bueno, G., Acloque, H., Vega, S., Barrallo-Gimeno, A., Cano, A., and Nieto, M.A. (2012). Metastatic colonization requires the repression of the epithelial-mesenchymal transition inducer Prrx1. Cancer Cell *22*, 709–724.

Oshimori, N., Oristian, D., and Fuchs, E. (2015). TGF-beta promotes heterogeneity and drug resistance in squamous cell carcinoma. Cell *160*, 963–976.

Pastushenko, I., Brisebarre, A., Sifrim, A., Fioramonti, M., Revenco, T., Boumahdi, S., Van Keymeulen, A., Brown, D., Moers, V., Lemaire, S., et al. (2018). Identification of the tumour transition states occurring during EMT. Nature *556*, 463–468.

Pattabiraman, D.R., and Weinberg, R.A. (2014). Tackling the cancer stem cells - what challenges do they pose? Nat. Rev. Drug Discov. *13*, 497–512.

Pierce, G.B., and Dixon, F.J., Jr. (1959). Testicular teratomas. I. Demonstration of teratogenesis by metamorphosis of multipotential cells. Cancer *12*, 573–583.

Prost, S., Relouzat, F., Spentchian, M., Ouzegdouh, Y., Saliba, J., Massonnet, G., Beressi, J.P., Verhoeyen, E., Raggueneau, V., Maneglier, B., et al. (2015). Erosion of the chronic myeloid leukaemia stem cell pool by PPARgamma agonists. Nature *525*, 380–383.

Puram, S.V., Tirosh, I., Parikh, A.S., Patel, A.P., Yizhak, K., Gillespie, S., Rodman, C., Luo, C.L., Mroz, E.A., Emerick, K.S., et al. (2017). Single-cell transcriptomic analysis of primary and metastatic tumor ecosystems in head and neck cancer. Cell *171*, 1611–1624.

Raghav, S.K., Waszak, S.M., Krier, I., Gubelmann, C., Isakova, A., Mikkelsen, T.S., and Deplancke, B. (2012). Integrative genomics identifies the corepressor SMRT as a gatekeeper of adipogenesis through the transcription factors C/EBPbeta and KAISO. Mol. Cell *46*, 335–350.

Rosen, E.D., Hsu, C.H., Wang, X., Sakai, S., Freeman, M.W., Gonzalez, F.J., and Spiegelman, B.M. (2002). C/EBPalpha induces adipogenesis through PPARgamma: a unified pathway. Genes Dev. *16*, 22–26.

Rosen, E.D., and Spiegelman, B.M. (2014). What we talk about when we talk about fat. Cell *156*, 20–44.

Samavarchi-Tehrani, P., Golipour, A., David, L., Sung, H.K., Beyer, T.A., Datti, A., Woltjen, K., Nagy, A., and Wrana, J.L. (2010). Functional genomics reveals a BMP-driven mesenchymal-to-epithelial transition in the initiation of somatic cell reprogramming. Cell Stem Cell *7*, 64–77.

Sanchez-Vega, F., Mina, M., Armenia, J., Chatila, W.K., Luna, A., La, K.C., Dimitriadoy, S., Liu, D.L., Kantheti, H.S., Saghafinia, S., et al. (2018). Oncogenic signaling pathways in the cancer genome atlas. Cell *173*, 321–337.e10.

Suenaga, M., Kurosawa, N., Asano, H., Kanamori, Y., Umemoto, T., Yoshida, H., Murakami, M., Kawachi, H., Matsui, T., and Funaba, M. (2013). Bmp4 expressed in preadipocytes is required for the onset of adipocyte differentiation. Cytokine *64*, 138–145.

Tam, W.L., and Weinberg, R.A. (2013). The epigenetics of epithelial-mesenchymal plasticity in cancer. Nat. Med. *19*, 1438–1449.

Tiwari, N., Tiwari, V.K., Waldmeier, L., Balwierz, P.J., Arnold, P., Pachkov, M., Meyer-Schaller, N., Schubeler, D., van Nimwegen, E., and Christofori, G. (2013). Sox4 is a master regulator of epithelial-mesenchymal transition by controlling Ezh2 expression and epigenetic reprogramming. Cancer Cell *23*, 768–783.

Tontonoz, P., Hu, E., and Spiegelman, B.M. (1994). Stimulation of adipogenesis in fibroblasts by PPAR gamma 2, a lipid-activated transcription factor. Cell *79*, 1147–1156.

Tontonoz, P., Singer, S., Forman, B.M., Sarraf, P., Fletcher, J.A., Fletcher, C.D., Brun, R.P., Mueller, E., Altiok, S., Oppenheim, H., et al. (1997). Terminal differentiation of human liposarcoma cells induced by ligands for peroxisome proliferator-activated receptor gamma and the retinoid X receptor. Proc. Natl. Acad. Sci. U S A *94*, 237–241.

Tsai, J.H., Donaher, J.L., Murphy, D.A., Chau, S., and Yang, J. (2012). Spatiotemporal regulation of epithelial-mesenchymal transition is essential for squamous cell carcinoma metastasis. Cancer Cell *22*, 725–736.

Tseng, Y.H., Kokkotou, E., Schulz, T.J., Huang, T.L., Winnay, J.N., Taniguchi, C.M., Tran, T.T., Suzuki, R., Espinoza, D.O., Yamamoto, Y., et al. (2008). New role of bone morphogenetic protein 7 in brown adipogenesis and energy expenditure. Nature *454*, 1000–1004.

Valiente, M., Obenauf, A.C., Jin, X., Chen, Q., Zhang, X.H., Lee, D.J., Chaft, J.E., Kris, M.G., Huse, J.T., Brogi, E., et al. (2014). Serpins promote cancer cell survival and vascular co-option in brain metastasis. Cell *156*, 1002–1016.

Van Keymeulen, A., Lee, M.Y., Ousset, M., Brohee, S., Rorive, S., Giraddi, R.R., Wuidart, A., Bouvencourt, G., Dubois, C., Salmon, I., et al. (2015). Reactivation of multipotency by oncogenic PIK3CA induces breast tumour heterogeneity. Nature *525*, 119–123.

Waldmeier, L., Meyer-Schaller, N., Diepenbruck, M., and Christofori, G. (2012). Py2T murine breast cancer cells, a versatile model of TGFbeta-induced EMT in vitro and in vivo. PLoS One *7*, e48651.

Wang, Q.A., Scherer, P.E., and Gupta, R.K. (2014). Improved methodologies for the study of adipose biology: insights gained and opportunities ahead. J. Lipid Res. *55*, 605–624.

Wielenga, M.C., Colak, S., Heijmans, J., van Lidth de Jeude, J.F., Rodermond, H.M., Paton, J.C., Paton, A.W., Vermeulen, L., Medema, J.P., and van den Brink, G.R. (2015). ER-stress-induced differentiation sensitizes colon cancer stem cells to chemotherapy. Cell Rep. *13*, 490–494.

Zheng, X., Carstens, J.L., Kim, J., Scheible, M., Kaye, J., Sugimoto, H., Wu, C.C., LeBleu, V.S., and Kalluri, R. (2015). Epithelial-to-mesenchymal transition is dispensable for metastasis but induces chemoresistance in pancreatic cancer. Nature *527*, 525–530.

STAR★METHODS

KEY RESOURCES TABLE

REAGENT or RESOURCE	SOURCE	IDENTIFIER
Antibodies		
Rabbit monoclonal Anti-Adiponectin	Cell Signaling Technologies	Cat# 2789, RRID:AB_2221630
Mouse monoclonal Anti-α-SMA	Sigma Aldrich	Cat# F3777, RRID:AB_476977
Rabbit monoclonal Anti- C/EBPα	Cell Signaling Technologies	Cat# 8178P, RRID:AB_11178517
Rabbit monoclonal Anti-C/EBPβ	Abcam	Cat# ab32358, RRID:AB_726796
Rabbit monoclonal Anti-Cleaved Caspase-3	Cell Signaling Technologies	Cat# 9664, RRID:AB_2070042
Rat monoclonal Anti-CD31	BD Pharmingen	Cat# 550274, RRID:AB_393571
Mouse monoclonal Anti-ERK-1 / ERK-2, diphospho	Sigma Aldrich	Cat# M8159, RRID:AB_477245
Rabbit unknown clonality Anti-MAP Kinase (ERK-1, 351-368)	Sigma Aldrich	Cat# M7927, RRID:AB_260665
Rabbit monoclonal Anti-MHC class I	Abcam	Cat# ab52922, RRID:AB_881225
Mouse monoclonal Anti-GAPDH	Sigma Aldrich	Cat# G8795, RRID:AB_1078991
Mouse monoclonal Anti-GLUT4	Abcam	Cat# ab65267, RRID:AB_1140009
Rabbit unknown clonality Anti-Mapkapk2	Cell Signaling Technologies	Cat# 3042L, RRID:AB_2141314
Guinea-pig polyclonal Anti-Perilipin	Fitzgerald Industries International	Cat# 20R-PP004, RRID:AB_1288416
Rabbit monoclonal Anti-Perilipin	Cell Signaling Technologies	Cat# 9349S, RRID:AB_10621999
Rabbit polyclonal Anti-Phospho Histone H3 (PH3)	Millipore	Cat# 06-570
Rabbit monoclonal Anti-Phospho-Smad3	Cell Signaling Technologies	Cat# 9520, RRID:AB_2193207
Rabbit monoclonal Anti-Phospho-Mapkapk2	Cell Signaling Technologies	Cat# 3007S, RRID:AB_490938
Rabbit polyclonal Anti-Phospho-Tak1	Cell Signaling Technologies	Cat# 9339, RRID:AB_2140096
Rabbit monoclonal Anti-PPAR-gamma	Cell Signaling Technologies	Cat# 2443, RRID:AB_823598
Rabbit monoclonal Anti-Smad2/3	Cell Signaling Technologies	Cat# 8685, RRID:AB_10889933
Rabbit polyclonal Anti-Tak1	Cell Signaling Technologies	Cat# 4505, RRID:AB_490858
Goat polyclonal Anti-Vinculin	Santa Cruz	Cat# sc-7649, RRID:AB_2288413
Mouse monoclonal Anti-Yes-associated protein (YAP)	Santa Cruz	Cat# sc-101199, RRID:AB_1131430
Mouse monoclonal Biotin-Anti- H-2Kd	Biolegend	Cat# 116604
PE-conjugated streptavidin	eBioscience	Cat# 12-4317-87
Rabbit monoclonal Anti-human HLA-A	Abcam	Cat# ab52922
Mouse monoclonal Anti-E-cadherin	BD Bioscience	Cat# 610182
Biological Samples		
Patient derived xenograft (PDX)-human breast cancer sample	obtained from M. Bentires-Alj, DBM, Basel	(PMID:26479923; Gao et al., 2015) The PDX code is 3078 (breast cancer).
Chemicals, Peptides, and Recombinant Proteins		
BODIPY 558/568	Thermo Fisher	D3835
Human BMP2	Sigma Aldrich	B3555
SB431542	Sigma Aldrich	S4317
Trametinib	LC Laboratories	T-8123
Human TGFβ1	R&D systems	240-B
Rosiglitazone	AdipoGen	AG-CR1-3570-G001
PD98059	Selleckchem	S1177
Critical Commercial Assays		
Lipolysis Assay Kit	Abcam	ab185433
Adiponectin Mouse ELISA Kit	Abcam	ab108785
Click-iT EDU	Thermo Fisher	C10337

(*Continued on next page*)

Continued

REAGENT or RESOURCE	SOURCE	IDENTIFIER
Deposited Data		
RNA-seq data (EMT kinetic)	Gene Expression Omnibus (GEO)	GSE50612
RNA-seq data (MTΔEcad day 7 comparison)	Gene Expression Omnibus (GEO)	GSE118612
RNA-seq data (3T3-L1 adipogenesis) (Al Adhami et al., 2015)	Gene Expression Omnibus (GEO)	GSE50612
Experimental Models: Cell Lines		
Mouse: MTflEcad	Laboratory of G. Christofori	N/A
Mouse MTΔEcad	Laboratory of G. Christofori	N/A
Mouse: Py2T/ GFP-Py2T	Laboratory of G. Christofori	N/A
Mouse: 3T3-L1	Laboratory of B. Deplancke	N/A
Mouse: ZS-Green 4T1	Laboratory of G. Christofori	N/A
Human: MDA-MB-231 LM2 GFP	Laboratory of J. Massague	N/A
female $RAG2^{-/-}$;common γ $receptor^{-/-}$ (RSG)	in house breeding	N/A
female $NMRI^{nu/nu}$	Janvier, Le Genest-Saint-Isle, France	N/A
female NOD/Scid;common γ $receptor^{-/-}$ (NSG)	in house breeding	N/A
Oligonucleotides		
Pparγ2	GCTGTGAAGTTCA ATGCACTGG	GCAGTAGCTGCACGTGCTCTG
Adiponectin	TGTTCCTCTTAATC CTGCCCA	CCAACCTGCACAAGTTCCCTT
FABP4	GATGCCTTTGTGG GAACCT	CTGTCGTCTGCGGTGATTT
Cebpα	AAACAACGCAACGT GGAGA	GCGGTCATTGTCACTGGTC
Zeb1	GCCAGCAGTCATGATGAAAA	TATCACAATACGGGCAGGTG
Zeb2	GGAGGAAAAACGTGGTGAACTAT	GCAATGTGAAGCTTGTCCTCTT
Klf4	CGGGAAGGGAGAAGACACT	GAGTTCCTCACGCCAACG
Snail1	CTCTGAAGATGCACATCCGAA	GGCTTCTCACCAGTGTGGGT
siControl	Ambion	4390846
siZeb1	Ambion	s74841
siZeb2	Ambion	s76954, s76956
siKlf4	Ambion	s68835, s68836, s68837
siSnail1	Ambion	s74062
Software and Algorithms		
R	The R Project for Statistical Computing	R_3.3.3
Bioconductor	https://www.bioconductor.org/	Bioconductor packages
STAR: ultrafast universal RNA-seq aligner	http://code.google.com/p/rna-star/	STAR
COMBAT	https://www.bu.edu/jlab/wp-assets/ComBat/Abstract.html	
IMARIS Software Imaris x64 9.1.2,	Bitplan, Concord, MA	N/A

CONTACT FOR REAGENT AND RESOURCE SHARING

Further information and requests for resources and reagents should be directed to and will be fulfilled by the Lead Contact, Gerhard Christofori (gerhard.christofori@unibas.ch).

MDA-MB 231 LM2 GFP were obtained from J. Massague via an MTA with Memorial Sloan Kettering Cancer Center, New York.

EXPERIMENTAL MODEL AND SUBJECT DETAILS

Cell Lines and Cell Culture

Py2T (Waldmeier et al., 2012), MTflECad, MTΔECad (Fantozzi et al., 2014), and ZsGreen 4T1 (Diepenbruck et al., 2017) were generated in the laboratory of G. Christofori (University of Basel) and previously described. MDA-MB-231 LM2 GFP (Kim et al., 2009) were

obtained from J. Massague (Memorial Sloan Kettering Cancer Center, New York, NY, USA) and 3T3-L1 cells (Green and Kehinde, 1975; Gubelmann et al., 2014) were obtained from B. Deplancke (EPFL, Lausanne). Cells were cultured in Dulbecco's modified eagle medium (DMEM; Sigma-Aldrich) supplemented with fetal calf serum (FCS, 10%; Sigma-Aldrich), glutamine (2 mM; Sigma-Aldrich), penicillin (100 U; Sigma-Aldrich) and streptomycin (0.2 mg/l; Sigma-Aldrich). All cell lines were grown at 37°C, 5% CO_2, 95% humidity.

Mice

All animal experiments have been performed under approval by the Kantonales Veterinäramt Basel-Stadt under permit numbers 1878, 1907 and 1908.

2-3 months old female RAG2$^{-/-}$;common γ receptor$^{-/-}$ (RSG), NMRI nu/nu, or NOD-Scid;common γ receptor$^{-/-}$ (NSG) mice were used for tumor transplantation experiments. No statistical methods were used to predetermine sample size. For all experiments presented in this study, the sample size was large enough to determine statistically significant effects. Once transplanted tumor cells formed palpable tumors, mice were randomized and allocated to different treatment groups. The investigators were not blinded to allocation during the experiments, yet they were blinded to allocation during the outcome assessment. The mouse colony was housed in a certified animal facility with a 12 hr light/dark cycle in a temperature-controlled room (22 ± 1°C) with free access to water and food, in accordance with Swiss guidelines.

Human Material

The patient-derived xenograft transplantation (PDX) mouse model of metastatic human breast cancer, described and characterized as x-3078 in (Gao et al., 2015), was kindly provided by M. Bentires-Alj, DBM, University of Basel, Switzerland.

METHOD DETAILS

In Vitro Adipogenesis

Cells were seeded at density of 20,000 cells/cm^2 and incubated overnight at 37°C in 5% CO_2. To induce differentiation of 3T3-L1, the growth medium was replaced with medium containing 5 μg/ml insulin, 1 μM Dexamethasone (dissolved in ethanol), 2 μM Rosiglitazone (dissolved in DMSO) for 48 hr, then in medium containing 5μg/ml insulin for 48 hr, then in medium containing 1 μM Rosiglitazone. To induce differentiation in cancer cells, cells were seeded and incubated overnight and then treated with 200 ng/ml human recombinant BMP2 (Sigma, B3555) for 3 days, with 200 ng/ml BMP2 and 2μM Rosiglitazone (Rosi) for 4 days, and with medium containing 2 μM Rosiglitazone for another 3 days. The addition of other growth factors or inhibitors is indicated in the figures, from day 0 to day 7 such as human recombinant TGFβ1 (R&D Systems, 240-B) at 2 ng/ml, and the MEK inhibitors PD98059 at 40 μM and Trametinib as indicated, and the TGFβ receptor 1 inhibitor SB431542 at 10 μM. Control cells were treated with medium containing DMSO.

In Vitro Chondrogenesis

Cells were seeded at a density of 60,000 cells/cm^2 in normal growth medium (DMEM supplemented with glutamine, penicillin, streptomycin and 10% FBS) and incubated at 37°C in 5% CO_2 overnight. Medium was removed and cells were washed with serum free Opti-MEM media (to remove traces of serum). Differentiation medium: Opti-MEM serum free media (Gibco) containing 1% ITS (BD), 10 μM Dexamethasone (Sigma Aldrich), 100 μM Ascorbate (Sigma Aldrich) and 10 ng/ml human recombinant TGFβ1. One day later, medium was removed, and cells were washed. From day 2 to day 21, differentiation medium was replaced every 48 hr with medium containing 10 ng/ml human recombinant BMP2 and BMP4. For control cells, normal culture medium was used.

In Vitro Osteogenesis

Cells were seeded at density of 20,000 cells/cm^2 in normal growth medium (DMEM supplemented with glutamine, penicillin, streptomycin and 10% FBS) and incubated at 37°C in 5% CO_2 for 48 hr. From day 2 until day 21 differentiation medium was used: Supplemented DMEM containing 1mg/ml β-Glycerophosphate (Calbiochem), 100 nM Dexamethasone and 100 μM L-Ascorbate, 1mM Sodium Pyruvate (Sigma) and 10ng/ml human recombinant BMP4 was added at each time point. Control cells were incubated with culture medium.

RNA Isolation and RT-PCR

Total RNA was prepared using TriReagent (Sigma-Aldrich) for cells or RNeasy mini kit (74104, Qiagen) for tissues. For RNA sequencing, total RNA was isolated using the miRNeasy mini kit (217004, Qiagen). RNA was reverse transcribed with M-MLV reverse transcriptase (Promega), and transcripts were quantified by PCR using SYBR-green PCR MasterMix (Invitrogen). Riboprotein L19 primers were used for normalization. PCR assays were performed in triplicate, and fold induction was calculated using the comparative Ct method (ΔΔ Ct). Primers used for quantitative RT-PCR are listed in the Key Resources Table.

Immunoblotting

Cells were lysed in boiling lysis buffer (0.29 M Tris-HCl pH 6.8, 4.7% SDS, 23% glycerol). Protein concentration was determined using the BCA assay kit (Pierce). Equal amounts of protein were diluted in SDS-PAGE loading buffer (10% glycerol, 2% SDS, 65 mM Tris, 1 mg/100 ml bromophenol blue, 1% β-mercaptoethanol) and resolved by SDS-PAGE. Proteins were transferred to nitrocellulose,

0.45 μM pore size membranes by wet transfer, blocked with 5% skim milk powder in TBS/0.05% Tween 20 and incubated with the antibodies indicated. HRP-conjugated secondary antibodies were detected by chemiluminescence using a Fusion Fx7 chemiluminescence reader (Vilber Lourmat, France).

siRNA Transfection

20 nM siRNAs (Ambion) against Zeb1 (s74841), Zeb2 (s76954, s76956 10nM each), Klf4 (s68835, s68836, s68837 6.66nM each), Snail1 (s74062) or a negative control (4390846) were prepared using Lipofectamine RNAiMax (Invitrogen) for the transfection according to the manufacturer's instructions. Cells were seeded and incubated with siRNA. After 24 hr (day 1) medium was changed to medium containing BMP2 (treated) or normal medium (no treatment) according to *in vitro* adipogenesis protocol. 48 hr later (day 3) medium was changed to adipogenesis or control medium and siRNA transfection was repeated. Cells were harvested at day 5.

Adiponectin Secretion

Supernatants of untreated cells (day 0) as well as control-treated cells and cells treated with the adipogenesis protocol for 10 days were harvested. Adiponectin concentrations were determined using the Adiponectin Mouse ELISA Kit (ab108785, Abcam) according to the manufacturer's protocol.

Lipolysis Analysis

Lipolysis was induced using Isoproterenol (final concentration 100 nM) in untreated cells (day 0) as well as in control-treated cells and cells treated with the adipogenesis protocol for 10 days. Glycerol release was measured using a Lipolysis Assay Kit (Colorimetric) (ab185433, Abcam) according to the manufacturer's protocol.

Extracellular Metabolic Flux Analysis

For analysis of metabolic signatures, a Seahorse XFe-96 metabolic extracellular flux analyzer was used (Seahorse Bioscience, North Billerica, MA, USA). Adipogenesis-treated (10 days) and undifferentiated control cells were used for metabolic analysis. Prior to performing the metabolic assays, differentiation media was exchanged with serum-free, unbuffered basal medium supplemented with 25 mM glucose and 2 mM glutamine (Seahorse, MA, USA). Mitochondrial perturbation profiling was used to determine mitochondrial respiratory and glycolytic parameters by sequential addition of oligomycin (1 μM), Carbonyl cyanide-4- (trifluoromethoxy)phenylhydrazone (FCCP) (0.6 μM), and rotenone/antimycin A (1 and 2 μM, respectively). Metabolic parameters were calculated as previously described (Gubser et al., 2013).

GLUT4 Translocation

Control cells and cells treated with the adipogenesis protocol were incubated for 25 min with 100 nM insulin or normal growth medium and subsequently visualized for the expression and localization of GLUT4 by confocal microscopy (Leica SP5).

EdU Incorporation to Detect Proliferating Cells

Cells before and after a full ten-day adipogenesis protocol were incubated for 24 hr with 1 μM EdU (Invitrogen) or 72 hr with 0.1μM EdU. Cells were fixed with 4% PFA for 20 min, washed with PBS, permeabilized with 0.5% NP40 and washed with PBS-T (PBS with 0,01% TX-100). ClickIT reaction was performed according to the manufacturer's protocol (BaseClick), cells were washed with PBS-T and used for immunostaining. Images were acquired with a fluorescence Leica DMI 4000 microscope. For each replica, at least 7 fields were quantified using intensity quantification function in ImageJ software.

Immunofluorescence Microscopy Analysis Cells

Cells were fixed with 4% PFA and permeabilized with 0.5% NP40. Cells were blocked with 3% BSA and incubated with primary antibody for 1.5 hr at room temperature or overnight at 4°C. After washing, cells were incubated with secondary antibodies for 1 hr at room temperature, washed and incubated with DAPI for 10 min, and washed and mounted with fluorescent mounting medium (Dako). Samples were imaged with a confocal microscope (LSM 510 Meta, Zeiss or Leica SP5) or with a fluorescence microscope (Leica DMI 4000). Cells expressing C/EBPα (Cat# 8178P) were manually quantified with ImageJ software for at least 5 fields per replica.

RNA Sequencing Analysis

Total RNA was isolated from cells of two independent experiments using the RNeasy Mini Kit (Qiagen) according to the manufacturer's instruction. RNA quality control was performed with a fragment analyzer using the standard or high sensitivity RNA analysis kit (DNF-471-0500 or DNF-472-0500) from Labgene and RNA concentration was measured by using the Quanti-iT^{TM} RiboGreen RNA assay kit (Life Technologies/Thermo Fisher Scientific). 200 ng of RNA was utilized for library preparation with the TruSeq Stranded Total RNA LT Sample Prep Kit (Illumina). Poly-A$^+$ RNA was sequenced by HiSeq SBS kit v4 (Illumina) on an Illumina HiSeq 2500 using protocols defined by the manufacturer.

Obtained single-end RNA-seq reads (63-mers) were mapped to the mouse genome assembly, version mm10, with RNA-STAR (Dobin et al., 2013), with default parameters except for allowing only unique hits to genome (outFilterMultimapNmax=1) and filtering reads without evidence in spliced junction table (outFilterType="BySJout"). Using RefSeq mRNA coordinates from UCSC (genome.

ucsc.edu, downloaded in December 2015) and the qCount function from QuasR package (version 3.12.1), we quantified gene expression as the number of reads that started within any annotated exon of a gene. The differentially expressed genes were identified using the edgeR package (version 1.10.1). Genes with FDR smaller than 0.05 and minimum log2 fold change of +/- 1 were used for downstream analysis.

Comparative Analysis

We compared our RNA-sequencing data with already published RNA-sequencing data obtained from 3T3-L1 cells (Al Adhami et al., 2015). The batch effects correction was performed on the gene expression data using ComBat (PMID: 16632515). We then computed spearman rank correlation coefficients between the data sets and the heatmap was generated using hierarchical clustering (hclust function) in heatmap2. All the above-mentioned computations were performed in R (R-3.3.1) version.

Regulatory Motif Analysis

Integrated System for Motif Activity Response Analysis (ISMARA) (PMID: 24515121) prediction tool was employed to identify regulatory motifs enriched in MTΔECad undergoing adipogenesis at different time points (0 hr, 6 hr, 3 days, 5 days, 7 days and 10 days) RNA-seq data. The data provided for ISMARA analysis was in FASTQ format and selected mm10 version as reference genome.

Functional Enrichment Analysis and Heatmaps

We performed functional enrichment analysis of differentially expressed genes for biological processes or pathways in R (3.3.1) using several publically available Bioconductor resources including GO.db (version 3.4.0), GOstats (version 2.40.0) (PMID: 17098774), KEGG.db (version 3.2.3) and ReactomePA (version 1.18.1) (PMID: 26661513). The significance of each biological processes or pathways identified was calculated using the hypergeometric test (equivalent to Fisher's exact test) and those with p values ≤ 0.05 were considered significant. Heatmaps were generated in R (3.3.1) using packages RColorBrewer (1.1-2) and gplots (3.0.1) using normalized CPM (counts per million) data obtained for RNA-sequencing experiments.

In Vivo Adipogenesis

For primary tumor transplantation experiments, $0.5x10^6$ GFP-expressing Py2T cells were injected into the mammary fat pad of female $RAG2^{-/-}$;common γ $receptor^{-/-}$ (RSG) mice. 2 weeks after injection, mice were treated daily with i.p injections of drugs or vehicle for two weeks. High dose group, 5 mg/kg PD98059 and 16 mg/kg Rosiglitazone dissolved in vehicle; low dose group, 2 mg/kg PD98059 and 16 mg/kg Rosiglitazone dissolved in vehicle; control group, vehicle alone (4% DMSO, 30% PEG300, 5% Tween 80).

For tumor invasion and metastasis experiments, female NMRI nu/nu mice were injected into the mammary fat pad with $0.5x10^6$ ZsGreen-expressing 4T1 cells and female NOD-Scid;common γ $receptor^{-/-}$ (NSG) mice were injected into the mammary fat pad with $1x10^6$ GFP-expressing MDA-MB-231 LM2 cells. MDA-MB-231 LM2 cells were obtained from J. Massague (Memorial Sloan Kettering Cancer Center, New York, NY, USA) and prepared separately with PBS 1:1 mix, and suspended with Cultrex (R) BME 2 RGF (ORGANOID MATRIX) PathClear (R)* (TRVIGEN/AMSBIO) before implantation.

After initial tumor growth, tumor volume was measured, and mice were divided into four treatment groups as follows: Group 1: Control treated with vehicle (0.5% hydroxypropyl methylcellulose and 0.2% Tween 80 in distilled water (pH 8.0) and 0.7% DMSO). Group 2: Rosiglitazone (20 mg/kg) dissolved in vehicle. Group 3: Trametinib (0.3 mg/kg) dissolved in vehicle. Group4: Rosiglitazone (20 mg/kg) and Trametinib (0.3 mg/kg) dissolved in vehicle. Mice were treated daily p.o. for three weeks. Animals were sacrificed, tumor volumes and weights were measured, and tumors and lungs were embedded in paraffin for H&E staining and OCT for immunofluorescence staining and frozen for protein isolation.

All studies involving mice have been approved by the Swiss Federal Veterinary Office (SFVO) and the Cantonal Veterinary Office of Basel Stadt (licenses 1878, 1907, and 1908).

PDX Human Breast Cancer Model

The patient-derived xenograft transplantation (PDX) mouse model of metastatic human breast cancer, described and characterized as x-3078 in (Gao et al., 2015), was kindly provided by M. Bentires-Alj, DBM, University of Basel, Switzerland. A tumor propagated in NSG female mice was dissected and cut in app. 1 mm^3 pieces. Tumor pieces were maintained in PBS until transplantation. 8-13 weeks-old NSG (female) mice were anesthetized with Isofluoran, and tumors were transplanted into the 9th mammary fat pad. The wounds were closed with metal clips, and the animals were placed under infrared light until full recovery. For pain relief, Meloxicam was administered (5 mg/kg body weight per day) for two days. Four weeks post-transplantation, the mice were divided into four cohorts and treatment was initiated as described (control, Rosiglitazone, Trametinib, and a combination of Rosiglitazone and Trametinib). Eight weeks post-transplantation, mice were anesthetized with Isofluoran, and tumors were surgically removed, measured and embedded in paraffin and OCT. Mice recovered for five days prior to treatment continuation. Animal health was monitored daily. Four months post-transplantation, mice were euthanized, and lungs isolated and embedded in paraffin for H&E staining and OCT for immunofluorescence staining.

Immunofluorescence Microscopy Analysis Tissues

Tumors were fixed in 4% PFA for 2 hr followed by overnight incubation in 20% sucrose to cryopreserve the tissue, both at 4°C. Then, tumors were snap frozen in Tissue-Tek OCT compound (Thermo Scientific) and stored at -80°C. 7 μm thick tumor sections were cut,

dried for 30 min, rehydrated with PBS, permeabilized with 0.2% Triton X-100 for 20 min and blocked with 5% normal goat serum (NGS; Sigma-Aldrich) for 1 hr. As an exception, when performing stainings with anti-cCasp3 antibodies, blocking was performed using 20% NGS. Subsequently, primary and secondary antibodies were diluted in blocking solution and incubated overnight at 4°C and 1 hr at room temperature, respectively. Nuclei were stained with 4′,6-Diamidin-2-phenylindol (DAPI; Sigma-Aldrich) followed by mounting the slides with Dako mounting medium (Dako).

For adipocyte images, 80 μm thick tumor sections were cut and treated as indicated previously with the exception of 2 hr blocking duration and 6 hr of secondary antibody staining.

For CD31, cleaved Caspase-3, PH3 and E-cadherin staining, images were acquired with a Leica DMI 4000 microscope. For Perilipin, $H2K^d$, HLA staining, images were taken with a confocal spinning disc microscope with CFI Plan Apo 20x, 0.75 NA objective lens (Nikon) with VisiView software (Visitrion). 3D reconstruction images were generated using Imaris' Surface function (Imaris x64 9.1.2).

Blood Vessel Density

To determine blood vessel density, $CD31^+$ vessels were quantified in 8-15 microscopic fields per tumor (depending on the tumor size) normalized to the respective tumor area.

Cell Proliferation and Apoptosis

Areas of cells positive for phospho-histone 3 (PH3; proliferating cells) or cleaved caspase-3 (cC3; cells undergoing apoptosis) were quantified in 8-20 microscopic fields per tumor (depending on the tumor size) and were normalized to the respective area of Zs-Green positive tumor cells.

Lung Metastasis Quantification

Histological lung sections were stained with hematoxylin and eosin (H&E) and imaged using an Axio Imager scanning microscope (Zeiss), and the number of lung metastasis per section was quantified using VIS software (Visiopharm https://www.visiopharm.com).

BODIPY Staining on Frozen Sections

Cryosections (7 μm or 80 μm thick) were rehydrated in PBS and incubated with BODIPY in the dark at room temperature for 30 min. Sections were washed and incubated with DAPI for 10 min, then washed and mounted with fluorescent mounting medium (Dako). Images were taken by laser scanning confocal microscopy (Leica SP5). Representative images for adipocytes expressing GFP were prepared with IMARIS 8.2.1 software.

Tumor Invasion and Adipocyte Quantification

Tumor frozen sections were stained with Perilipin (Fitzgerald Industries International, Cat# 20R-PP004) and DAPI, PDX-tumors were stained with HLA (MHC class I, Abcam, Cat# ab52922) followed by imaging the complete section using a confocal spinning disc microscope (Visitron). Quantifications were performed using Arivis Vision4D software. For invasiveness analysis, the borders of tumor to mammary gland tissue were defined and 1 mm^2 quantification boxes were located. In each box, the tumor bulk and the tumor invasive areas were identified and analyzed for HLA-A-expressing or GFP-positive cancer cells. The percentage of invasive front of the total tumor border area was calculated and quantified. The co-staining of GFP or HLA-A-positive cells with Perilipin was used to quantify cancer cell-derived adipocytes.

QUANTIFICATION AND STATISTICAL ANALYSIS

Data is presented as mean ± SEM. Statistical analysis and graphs were generated using R software and GraphPad Prism software. Statistical analysis was performed as indicated in the figure legends. *In vitro* studies were biologically repeated at least three times unless otherwise specified, and statistical analysis was performed using unpaired t-test. The numbers of animals in each experiment are indicated in the figure legends. For tumor growth curves, linear regression was calculated and statistical difference between the groups was calculated using mean-t statistic and p value adjustment based on the Holm-Bonferroni method. All other *in vivo* statistical analysis was performed using Kruskal-Wallis test corrected for multiple comparisons unless stated otherwise in figure legends.

In vitro experimental procedures were compared to control, *in vivo* the various treatments were compared as indicated, with a significance indication: p values (GP style): *, $p < 0.0332$; **, $p < 0.0021$; *** $p < 0.0002$; ****, $p < 0.0001$; ns, non-significant.

DATA AND SOFTWARE AVAILABILITY

The RNA sequencing data of MTΔECad mesenchymal breast cancer cells undergoing adipogenesis into terminally differentiated adipocytes are deposited at Gene Expression Omnibus (GEO accession number: GSE89553). The RNA sequencing data of MTΔECad and Py2T-LT treatment comparison at day 7 are deposited at Gene Expression Omnibus (GEO accession number: GSE118612).